Forschungszentrum Karlsruhe
in der Helmholtz-Gemeinschaftt

Wissenschaftliche Berichte
FZKA 7214
SAM-LACOMERA-D15

The COMET-L2 Experiment on Long-Term MCCI with Steel Melt

G. Sdouz, R. Mayrhofer, H. Alsmeyer, T. Cron, B. Fluhrer, J. Foit, G. Messemer, A. Miassoedov, S. Schmidt-Stiefel, T. Wenz

Institut für Kern- und Energietechnik
Programm Nukleare Sicherheitsforschung

Juni 2006

Forschungszentrum Karlsruhe

in der Helmholtz-Gemeinschaft

Wissenschaftliche Berichte

FZKA 7214

SAM-LACOMERA-D15

The COMET-L2 Experiment on Long-Term MCCI with Steel Melt

G. Sdouz*, R. Mayrhofer*, H. Alsmeyer, T. Cron, B. Fluhrer, J. Foit, G. Messemer, A. Miassoedov, S. Schmidt-Stiefel, T. Wenz

Institut für Kern- und Energietechnik

Programm Nukleare Sicherheitsforschung

*ARC Seibersdorf research GmbH, Austria

Forschungszentrum Karlsruhe GmbH, Karlsruhe

2006

Forschungszentrum Karlsruhe GmbH
Postfach 3640, 76021 Karlsruhe

Mitglied der Hermann von Helmholtz-Gemeinschaft
Deutscher Forschungszentren (HGF)

ISSN 0947-8620

urn:nbn:de:0005-072140

ABSTRACT

Former results in the molten-core-concrete interaction (MCCI) research indicate a possible penetration of a PWR cavity during a severe accident. To investigate the coolability of molten core the COMET facility was commissioned. The LACOMERA project is a 3 year shared-cost action within the Fifth Framework Programme. The overall objectives of the LACOMERA project are to provide research institutions from the EU member countries and associated states access to large scale experimental facilities which shall be used to increase the knowledge of the quenching of a degraded core and regaining melt coolability in the reactor pressure vessel, of possible melt dispersion to the cavity, of MCCI and of ex-vessel melt coolability.

The experiment COMET-L2 is designed to answer following questions: investigation of long-term MCCI of metallic corium in cylindrical siliceous concrete cavity under dry conditions with decay heat simulation of intermediate power during test phase 1, and subsequently at reduced power during test phase 2. Observation of downward and sideward cavity erosion rates, cavity shape, and related processes.

The experiment is performed in a cavity of siliceous concrete, initial inner diameter 595 mm. The mass of the metal melt is 430 kg, overlaid by 35 kg oxide melt. Decay heat was simulated by induction heating of the metal phase with a typical power of 200 kW, representing accident conditions in the late ex-vessel phase. Erosion of the concrete, temperatures of the melt, and erosion rates are measured. Unfortunately, the gas measurement system failed. In the first phase of the interaction, initial overheat of the melt is quickly reduced, while erosion rates into the axial and lateral directions are similar. When stationary conditions are achieved, the axial erosion seems more pronounced. Reasons for the differences between axial and radial erosion following the initial transient phase, and notably also the local inhomogeneities in axial ablation, may lie in the melt heating by a planar induction coil. This technique could possibly have resulted in inhomogeneous distribution of power in the melt, with a larger proportion close to the axial ablating concrete thus promoting axial ablation. The axial ablation might have been further amplified by possible positive feedback due to progression of the erosion front towards the coils, which eventually led to the cone-shaped erosion profile.

Details of the experiment are reported to be used for validation of models and computer codes for safety assessment.

ZUSAMMENFASSUNG

Das COMET-L2 Experiment zur Langzeiterosion von Beton durch einer Metallschmelze

Frühere Ergebnisse bei der Untersuchung von Beton-Schmelze-Wechselwirkung (MCCI) können ein mögliches Durchdringen eines Druckwasserreaktor – Betonfundaments nicht ausschließen. Zur Untersuchung der Kühlbarkeit von Kernschmelzen im Fundamentbereich wurde die COMET Anlage errichtet. Um Mitgliedern der EU den Zugang zu Versuchsanlagen zu ermöglichen, wurde im 5.Rahmenprogramm die Shared Cost Action LACOMERA (LArge scale experiments on COre degradation, MElt Retention And coolability) durchgeführt.

Das Experiment COMET-L2 untersucht im Wesentlichen folgende offenen Fragen: Untersuchung der langzeitigen MCCI einer metallischen Schmelze in einer zylindrischen Betonkaverne ohne Anwesenheit von Wasser mit einer Simulation der Nachzerfallswärme mittlerer Leistung während der Testphase 1. In der zweiten Phase wurde die Leistung reduziert. Im weiteren Beobachtung von axialer und radialer Erosion in der Kaverne, deren Form und damit in Zusammenhang stehende Phänomene.

Das Experiment wird in einer Kaverne mit einem Anfangsdurchmesser von 595 mm durchgeführt, gefertigt aus Beton mit silikatischen Zuschlägen. Die Schmelze besteht aus 430 kg Metall, überschichtet von 35 kg Oxidschmelze. Die nukleare Nachwärme wird durch induktive Beheizung der Metallphase simuliert, mit einer typischen Leistung von etwa 200 kW. Dies stellt die Unfallbedingungen in der späten Phase der Fundamenterosion dar. Es werden die Erosion des Betons und die Temperaturen der Schmelze gemessen. Leider versagte die Anlage zur Gasmessung von Beginn an. In der ersten Phase der Wechselwirkung mit dem Beton beobachtet man eine schnelle Abnahme der Temperatur der Schmelze, bei etwa gleichen Erosionsraten nach unten und zur Seite. Nach Erreichen von nahezu stationären Bedingungen scheint die Erosion nach unten vorzuherrschen. Die Gründe für diese Unterschiede zwischen radialer und axialer Erosion und den lokalen Inhomogenitäten in axialer Richtung liegen möglicherweise in der Erwärmung durch eine induktive Heizung. Diese Technik ist vermutlich verantwortlich für eine inhomogene Verteilung der Leistung in der Schmelze und bevorzugt die axiale Erosion. Dieser Effekt wird bei der Annäherung der Erosionsfront an die Spule verstärkt, und ruft das kegelförmige Erosionsprofil hervor.

Die Einzelheiten des Experiments werden berichtet. Sie können verwendet werden, um Modelle und Rechenprogramme zur Sicherheitsanalyse von Reaktoren zu validieren.

TABLE OF CONTENTS

LIST OF TABLES

LIST OF FIGURES

1 Introduction

The LACOMERA project at the Forschungszentrum Karlsruhe, Germany is a 4 year action within the 5th Framework Programme of the EU which started in September 2002 [1]. Overall objective of the project is to offer research institutions from the EU member countries and associated states access to four large scale experimental facilities QUENCH, LIVE, DISCO, and COMET which can be used to investigate core melt scenarios from the beginning of core degradation to melt formation and relocation in the vessel, possible melt dispersion to the reactor cavity, and finally corium concrete interaction and corium coolability in the reactor cavity. In all experiments, simulant material is used to investigate the behaviour of the core material. These simulant materials were especially chosen to be as close to the real core material for the important properties as possible. On the other hand, the use of the simulant material allows covering a wide and broad range of scenarios with the experiments in a relatively small time schedule and for relatively low budget/funding. The experiments, as well as necessary post test investigations and special effect tests can be performed under well defined conditions and can be completely controlled.

The focuses of this project are large scale tests under prototypical conditions. This helps in the understanding of core degradation and quenching, melt formation and relocation as well as melt coolability in real reactors in two ways – firstly directly by scaling-up and secondly indirectly by providing data and models for the improvement and validation of computer codes. The large scale of the experiments allows extrapolation to the reactor case. Moreover, the flexibility and variability of the facilities is high due to the rather simple handling. These tests can be seen as complementary to tests with UO_2 in other research centres.

COMET-L2 was planned to fulfil the proposals of ARC Seibersdorf research GmbH [2], Austria. The experiment is designed to answer following questions: investigation of long-term MCCI of metallic corium in cylindrical siliceous concrete cavity under dry conditions with decay heat simulation of intermediate power during test phase 1, and subsequently at reduced power during test phase 2. Observation of downward and sideward cavity erosion rates, cavity shape, and related processes. The test uses a heated metal melt that is covered by an inevitable small oxide layer. Decay heat is simulated in the metal melt by electrical inductive heating.

With the experience from the previous COMET-L1 experiment [7], special considerations are given to the rating of internal heating of the melt, which simulates the nuclear decay heat by induction heating of the metal phase. The power, which can be transferred by induction

heating, is limited by the relatively small electromagnetic efficiency of the induction coil, which is strongly reduced for thicker basements. The goal is, to avoid the formation of a stable interface crust in phase 1 of the test by supplying sufficient decay power, and to observe the onset of possible crust formation and its consequences when in phase 2 of the test the simulated decay power is reduced.

This experiment is complementary to the present OECD-CCI tests that are carried out at ANL with pure oxidic corium (Farmer [3]), and to the large scale, transient ECOKATS-2 experiment (Alsmeyer [4]).

The report gives a description of the COMET facility and the operating systems, as well as a presentation and analysis of the test results. The experiment was conducted on February 5th, 2005. A short overview of the main test parameters is provided in Table 1.

Table 1: Specifications for COMET-L2

Parameter	**Specification**
Corium simulant	Metal (Fe + Ni) and oxide (Al_2O_3 + CaO)
Melt formation	Thermite reaction
Initial temperature of the melt	1750 to 1800°C
Initial melt mass	430 kg metal + 35 kg oxide
Radial erosion limit	250 mm
Axial erosion limit	170 mm
Concrete type	Standard siliceous concrete
Initial cavity dimension	D_i = 595 mm, H_i = 615 mm
Simulated decay heat	Induction heating at approx. 200-250 kW
Facility pressure	Atmospheric
Cover gas	Argon
Flow rate of the cover gas	50 m^3/h main flow and 2 x 8 m^3/h from windows
Criteria for phase 1	250 kW heating until 13 cm downward erosion during the dry phase
Criteria for phase 2	200 kW heating until 17 cm
Criteria for test termination	1) Contact of the melt with a light guide 2) 25 cm radial erosion 3) Porous concrete at the bottom reached

2 COMET L2 test design

2.1 Facility description

The COMET test facility consists of a test rig with the concrete crucible, an external melt generator, induction heating system with power supply and power control, off-gas system, water supply, a series of measurement and video systems, and the data acquisition systems [5]. The schematic illustration with the main elements of the COMET test rig is shown in Figure 1. The COMET facility and the supporting systems are located in a dedicated building. Due to safety reasons the control room with the equipment for online measurements is located in a bunker next to this building.

The outer crucible consists of a composite protection tube that includes the large test insert, and is designed to withstand higher pressure pulses if they would occur. The test rig is located on a transport car to allow installation and disassembly of the facility.

The simulated corium melt is generated externally by a thermite reaction (see chapter 2.2) with an initial temperature of about 1800°C and poured into the crucible through a lid in the upper hood. This moment defines the experimental time zero, when the first phase of dry erosion starts. When the melt approaches the light guides at the bottom of the crucible the test will stop and flooding from the top is initiated. During the course of the test, continuous heating takes place through the induction coil located under the bottom concrete shell.

The outer crucible is gas tight, so all gases generated during the experiment, are collected in the free volume of the crucible and feed through the off-gas system into the ambient atmosphere. A constant argon cover gas flow is injected into the crucible to prevent the accumulation of a burnable gas mixture. In the off-gas system, the main characteristics such as temperature, composition and flow rate of the released gases are measured online.

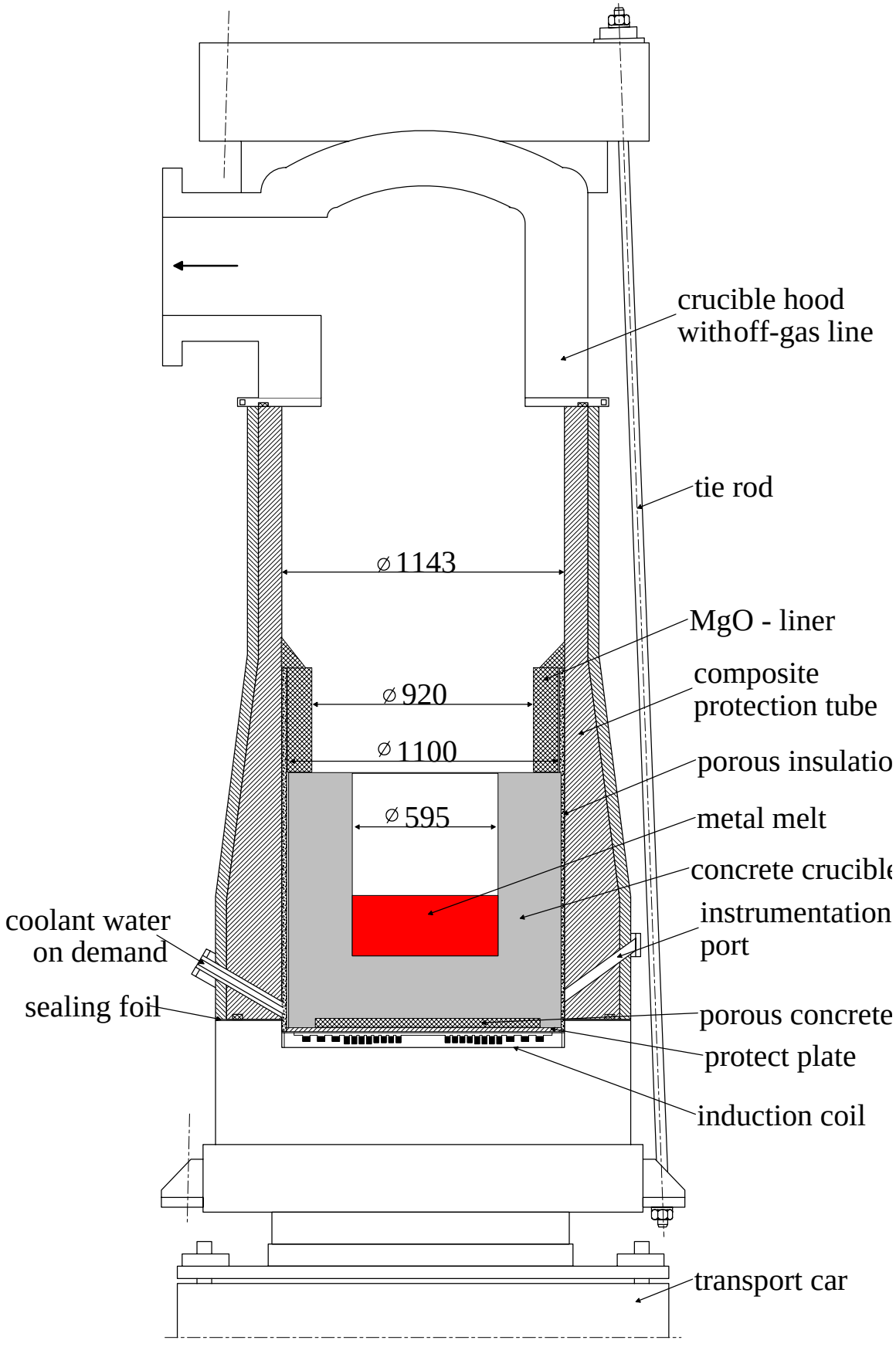

Figure 1: COMET test rig with its element

The induction coil, which supplies the electromagnetic 1000 cps heating power to the melt, is water-cooled. All other components located on the transport car are fabricated from non-metallic materials to exclude coupling to the induction field. The upper surface of the induction coil is covered by a 5 mm silicone foil, which protects the coil against any water that might be released from the concrete cavity. A 10 mm thin, refractory plate protects the induction coil, if hot melt would penetrate the concrete crucible. The distance between the induction coil and concrete crucible or melt respectively is kept as small as possible to reduce the inductive losses [6].

The crucible is fabricated from standard siliceous concrete. The composition of the concrete in weight percentages is as follows: SiO_2 70.3%, $Ca(OH)_2$ 13.55%, Al_2O_3 6.58%, $CaCO_3$ 5.46%, free H_2O 4.11%. The cement is of the type blast furnace cement CEM III/B 32,5 NW/HS.

The cylindrical ring of MgO oxide, located above the crucible, is 90 mm thick and has an inner diameter of 920 mm (Figure 2). The ring is stable enough so that the melt may attack only the structures below it. The gap between the ring and the protection tube is filled with coarse silica gravels used as a thermal insulation.

The inner structure of the composite protection tube is formed by refractory concrete and the outer shell of gas-tight, high temperature epoxy with glass fiber. The upper hood is a steel structure with inner ceramic liner and is connected to the off-gas tube. The role of the four tie rods is to tighten the upper and lower parts of the facility and maintain its integrity in case when inner mechanical loads act on the structure.

Two redundant water supply lines are connected to the porous concrete layer under the bottom of the crucible, to which water may be supplied on demand (Figure 2). This layer shall act as an efficient heat sink when later in the test the melt has propagated to the lower bottom of the inner concrete crucible, and the residual heat from concrete and melt must be removed to maintain the integrity of the induction heating system. Two instrumentation ports to the lower concrete cavity are used for thermocouple and light guides instrumentation of the crucible.

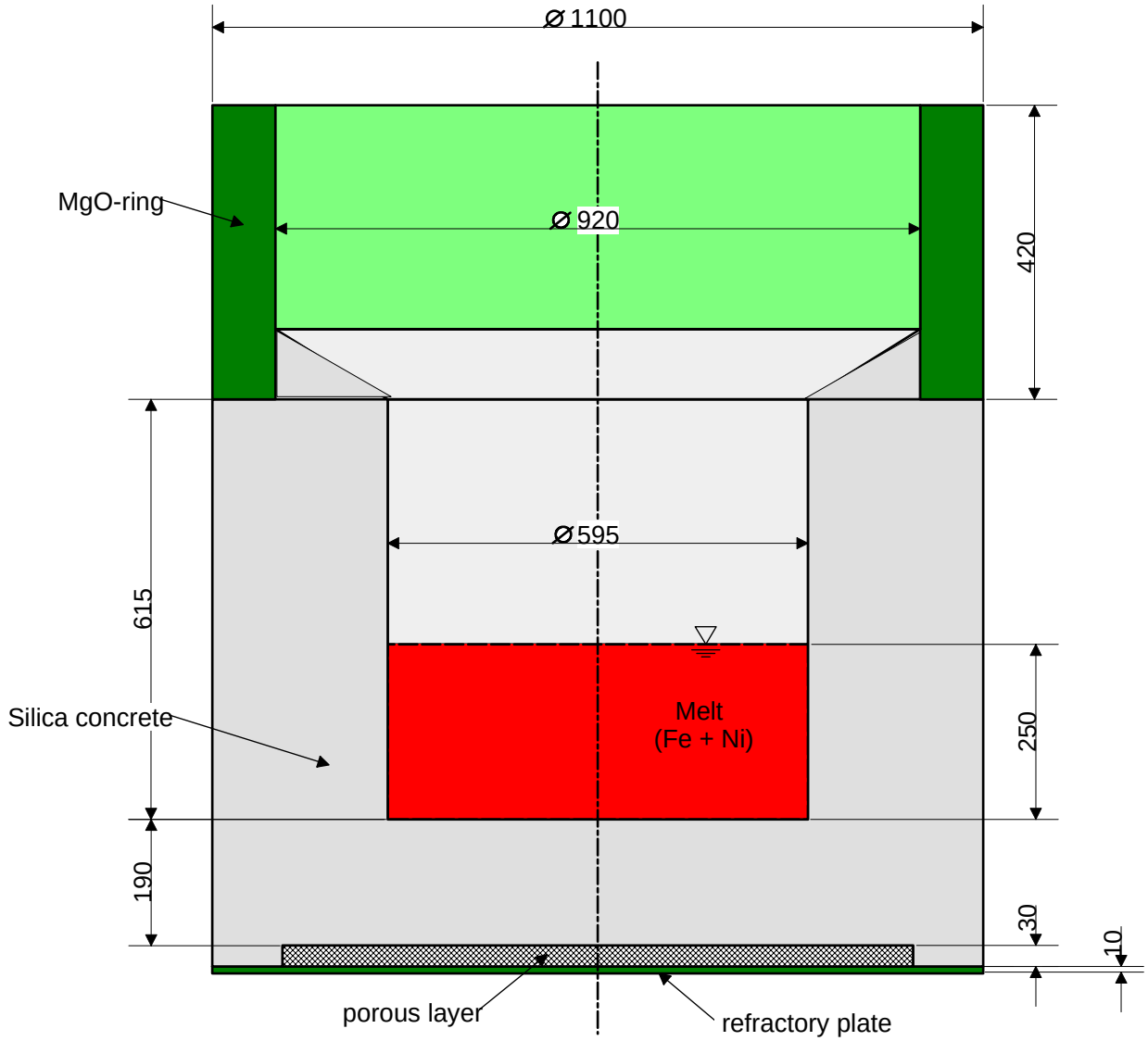

Figure 2: Dimensions of COMET-L2 crucible

To allow sufficient time and material for the erosion process, the cavity of the crucible is fabricated as a massive structure of siliceous concrete (Fig.2). The outer diameter is 1100 mm as limited by the COMET facility. The inner diameter was planned as 600 mm, to allow a maximal lateral erosion of 250 mm. The planned thickness of the bottom of the crucible is 180 mm, which limits the maximal downward erosion. This thickness is limited by the maximal distance to the induction coil, and shall allow supply of 250 kW net power to the melt. With respect to the preceding COMET-L1 test, the following modifications are important:

1 Heating efficiency: To increase the heating efficiency, we have reduced the thickness of the bottom of the concrete crucible, from 250 + 40 mm = 290 mm in COMET-L1 to 190 + 30 mm = 220 mm in COMET-L2. This should bring up the net power to ~ 250 kW.

2 Maintaining the power during the test: Power failure in COMET-L1 was due to electrical failure of a power control board and did not depend on the conditions of the L1 test. The

board was repaired and a complete check of the induction system was passed successfully. We expect that we are able to apply inductive heating until we reach the maximum allowed downward or lateral erosion.

The initial height of the metal phase is 250 mm, without taking into account the porosity of the melt by gas release. Some deviations from the inner cavity dimensions occurred due to deformation of the inner mold during fabrication of the crucible. Therefore, the following dimensions are changed:

1 The diameter of the inner cavity is 595 mm instead of 600 mm.
2 The thickness of the baseplate is 190 mm instead of 180 mm. This means that effectively the bottom and sidewalls of the inner cavity are covered by an additional concrete layer of 10 mm and 2.5 mm, respectively. Therefore the height of the crucible is 805 mm. The position of the thermocouples, embedded in the crucible remains unchanged referred to the central axis and the lower side of the concrete cylinder.

2.2 Melt generation and melt composition

With the given dimensions of the inner cavity, the mass of the metallic melt is selected to fill the cavity – without void – with 250 mm (Fig. 2). The steel height decreases during the test when radial cavity erosion proceeds. This means, that for a radial erosion from 600 mm to e. g. 900 mm the height of the steel is reduced to 44 %, that is from 250 mm to 111 mm. Initially, no oxide shall be present on top of the steel melt, but would build up due to accumulation of the concrete decomposition products throughout the test.

The required steel mass (Fe+Ni) for h = 25 cm is 460 kg with a liquid density of 6500 kg/m^3. The corresponding volume is 0.0707 m^3. The power densities, referred to the surface of the concrete surface which is in contact with the steel melt and referred to the volume of the metal melt, respectively, are given in Table 2 for a planned net input power to the melt of 250 and 200 kW in test phase 1 and 2, respectively

Table 2: Planned power densities in COMET-L2

P_{Netto}	Q_{Surf}	Q_{Vol}
Phase 1: 250 kW	332 kW/m²	3536 kW/m³
Phase 2: 200 kW	265 kW/m²	2829 kW/m³

The simulated corium melt is generated by a thermite reaction in a separate reaction vessel located above the test facility. The basis for this reaction is a thermite powder that provides liquid Al_2O_3 and iron by strongly exothermic reaction.

$$Al + Fe_2O_3 \rightarrow Al_2O_3 + Fe + h_{chem} \quad (1)$$

To guarantee safe release of the oxide fraction from the thermite vessel the solidification temperature of the oxide melt was reduced in adding burned lime CaO to the thermite powder. The resulting oxide is then a mixture of two oxide components (Al_2O_3 and CaO). For the steel melt, 10 w% Ni are added to the Fe melt, resulting in 460 kg Fe+Ni melt. Ni lowers the solidification range of the steel melt and represents components of the stainless steel of core structures. Furthermore, from the point of induction heating, Ni makes coupling to the induction field more stable if the steel temperature should strongly decrease and approach the Curie temperature. No further metals are added as they would no more exist in metallic form at that time of the accident for which this long-term MCCI experiment is representative (e.g. no Zr or Cr).

The thermite powder for the experiment is composed of two types of commercial powders, namely R 70 HC and Al SSH. Furthermore, steel in form of nails and the nickel pellets are added, which supply 40 % of the total metal melt.

Table 3 shows the composition of the thermite mix and of the resulting high temperature melts after completion of the thermite burn.

Table 3: Melt generation by thermite reaction in COMET-L2

Thermite mixture		**Produced melt**	
Thermite “Th”	555.85 kg	275.70 kg Fe	280.15 kg Al_2O_3
Fe pins	137.85 kg	137.85 kg Fe	-
Ni pellets	45.95 kg	45.95 kg Ni	-
CaO	83.68 kg	-	83.68 kg CaO
total	**823.33 kg mix**	**459.50 kg Fe+Ni**	**363.83 oxide**

After initiating of the thermite burn, the thermite reaction is normally completed within some 30 seconds. After additional 60 s for the metal and oxide melts to separate completely into the denser steel and the less dense oxide layer, melt pour starts: All metal is poured into the test crucible. When the weight loss of the thermite vessel indicates completion of the metal pour, the remaining oxide melt is directed into a slag wagon.

The initial temperature of the melt is expected with 1800°C. This is sufficiently high so that melt pour from the thermite vessel should occur without problem. To reach this temperature, preheating of the thermite powder mixture to about 200°C is performed in the thermite vessel.

2.3 Decay heat simulation

The simulation of the decay heat in the melt is achieved by induction heating which couples to the metallic fraction of the melt. The horizontal induction coil, located under the crucible, forms the resonance circuit together with a set of 27 high voltage capacitors driven by a 1 kHz power supply. The maximum inductor voltage is 2600 V; the maximum current is 12000 A. The equivalent rated upper heating power for a non-magnetic melt is 400 kW. The heating power deposited in the melt is determined online by the actual measured total power from which the losses by ohmic resistance and by the electromagnetic stray field are subtracted. These losses were determined in separate system tests, depending on voltage and currents of the induction circuit. In addition, a complete balance of all electric cooling circuits confirms the validity of this approach.

During the experiment, the inductive power is adjusted by control of the inductor voltage. This is performed manually by the operator, based on the displayed actual power history.

The net heating power may vary strongly with the coupling efficiency between induction coil and metal melt. All relevant data of induction heating are monitored for detailed evaluation. There are three processes influencing the electromagnetic coupling:

- Agitation and variation of the void in the melt: for higher void the efficiency of the coupling is reduced. Strong high frequency power oscillations are characteristic for the early MCCI processes. Solidification of the melt, in whatever structure, leads to more stable coupling.
- The reduced distance between melt and induction coil, which is a consequence of the concrete erosion, improves the coupling.
- The electrical properties of the metal melt change with temperature. The most important property for the actual melt is the magnetic permeability which increases strongly

below Curie temperature (400°C). This will occur after solidification of the melt and further cooling of the melt, resulting in a higher efficiency of heating.

In the present test, the induction heating system was started already 160 seconds before melt pouring. It was planned to reach ~250 kW of net power during the first phase of the experiment and to reduce the net power to ~200 kW during the second phase of the experiment.

2.4 Water supply and off-gas systems

The water for the supply system, to be activated later in the test, is provided from a water tank, located 2 m above the inner bottom surface of the crucible. The water level in the tank is kept constant by automatic level control and refill of fresh water from the building supply system. The temperature of the water is 20 C. The water system is controlled by the operator and the flow of the water can be modified.

The off-gas system is connected to the crucible through the hood. The system consists of a horizontal 1 m long tube with a ceramic liner of 400 mm inner diameter, a vessel to retain any melt which could be ejected from the test vessel, and an 11 m long horizontal steel tube with 500 mm inner diameter, exhausting the gas flow to the atmosphere outside of the building.

The large volume of the off-gas system excludes pressure build-up in the test vessel even for high gas rates. The off-gas system is preheated to 110°C before and during the experiment to exclude condensation of the steam. The end of the off-gas tube is closed in the beginning by a paper diaphragm, which allows argon inertisation before starting the test. This diaphragm is expelled by the first hot gases produced during pouring of the melt. Off-gas analyses are performed by instrumentation located along the off-gas tube, including a mass spectrometer for chemical analysis.

At the end of the off-gas tube, a heater plug ignites the off-gas if the concentration of the burnable gases is sufficient. A standing flame usually characterizes the first phase of dry concrete erosion when high amount of hydrogen is released [6].

2.5 Instrumentation and data acquisition

The COMET facility is equipped with a multitude of instrumentation to monitor and control the experiment and to collect data for subsequent evaluation. All data are stored and displayed on a PC data acquisition system as well as online registration using chart recorders and printers.

Moreover, several video systems are used to observe the experiment, including two video installations, which are directed from the crucible hood onto the surface of the melt. These systems are especially useful to observe all processes which are related to crust formation on the melt surface and during cooling. An infrared (IR) video camera was installed on top of the hood of the crucible, viewing through a sapphire window on the surface of the melt. This camera operates in the IR wavelength range from 3.4 to 5.0 μm and produces a video film. Additionally every 15 s, up to 240 high quality digital pictures are taken during 60 min. This allows determination of localized temperatures of the surface of the melt or of the upper crust throughout the experiment. As for any IR system, to derive the temperature or the emitted radiation from the surface, assumptions have to be made for the emissivity of the surface.

The measurement signals are collected to characterise the information written below:

- Electrical induction heating: Total power, net power, various voltages and currents, inductor frequency, control temperatures and coolant flows.
- Generation and pouring of the thermite melt: mass of the melt in the thermite reaction vessel, temperature of the melt during pouring, signals to control the pouring process.
- Coolant flow to the crucible: water flow rate, water pressure, height of water level during flooding.
- Upper crucible hood: temperature and pressure in the gas room, control and rate of the argon cover gas flow.
- Off-gas system: gas flow, temperature and pressure; gas composition by on-line quadrupole mass spectrometry.
- Control signals and conditions of the experimental hall.

Instrumentation of the crucible is given in Figure 3 - Figure 5. All indicated thermocouples are of the type NiCr-Ni. They fail at ~1350°C, and therefore operate until melting of the concrete does occur. Their failure indicates arrival of the melt front. These thermocouples are however unable to measure the temperature of the melt. Important is that the thermocouples give sufficient information during the test about the actual position of the melt front. Therefore, the instrumentation is arranged in two perpendicular planes, namely SW-NE and NW-SE, given in the overview of Figure 3 for easier comparison. The complete instrumentation of the planes SW-NE and NW-SE is shown in Fig. 4 and Fig. 5. The total number of NiCr-Ni thermocouples is 90. This number is limited by the high quality amplifiers which are required.

The positions of the thermocouples referred to the centreline and to the bottom of the cavity are listed in Table 4 and Table 5.

No thermocouples are installed to measure the temperature of the melt in the crucible during the erosion, because no stable thermocouples exist for this critical application. W-Re-thermocouples that were installed in the previous COMET-L1 test [7], failed very early in the test phase before showing any valid temperature because of the destruction by the very aggressive melt, especially because of the Fe content.

As we can not be sure to detect any critical position of the melt front by the thermocouples, additional safety relevant instrumentation in form of light guides is located in the outer sections of the crucible. It is planned to run the test until the melt approaches the light guides. If they are interrupted by the melt, heating is switched off immediately, and the melt cools down. To prevent further erosion by the solidifying melt during cool down and to exclude attack of the test rig, water will be supplied to the sidewall and/or to the bottom of the outer surface of the concrete crucible after end of heating. For this purpose, the bottom of the crucible has a 40 mm thick porous concrete layer which is flooded only after failure of the (bottom) light guides. Also the sidewall of the crucible is flooded through a gap that exists between the concrete crucible and the inner wall of the protection tube of the COMET facility. This gap is filled with silica gravels to be flooded on demand. Bottom flooding and sidewall flooding can be activated independently. Under the crucible, a protect plate, 10 mm thick, of refractory oxide material is located to protect the COMET induction coil in case that melt should penetrate through the bottom porous layer (Fig. 2).

During pour of the melt, its initial temperature will be measured in the spout. This is a well-established, reliable technique.

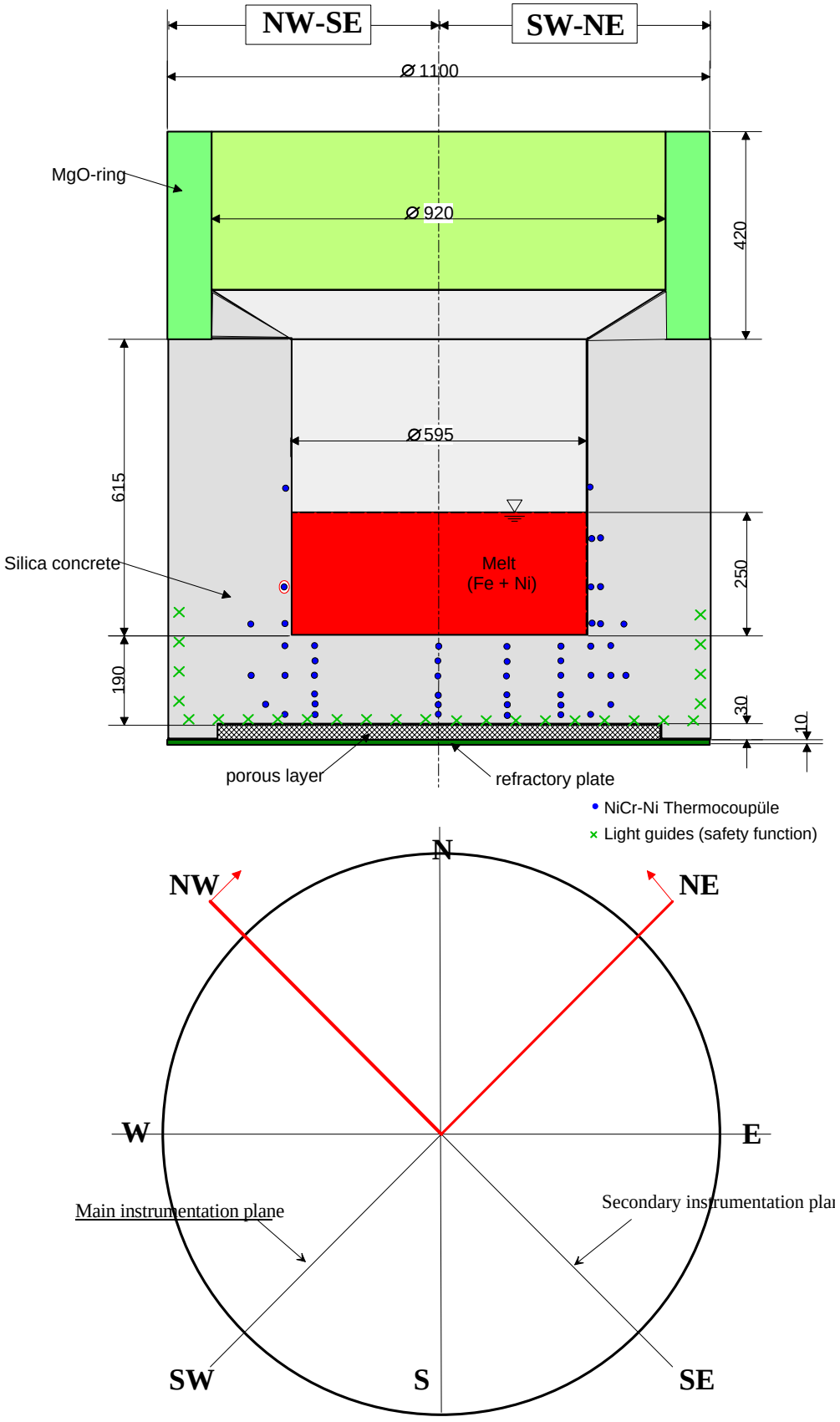

Figure 3: Thermocouple instrumentation in planes NW-SE and SW-NE (overview)
right side: main instrumentation plane, representing left and right side of plane SW-NE
left side: secondary instrumentation plane, representing left and right side of plane NW – SE
x indicates light guides which switch off the decay heat simulation when interrupted by the melt

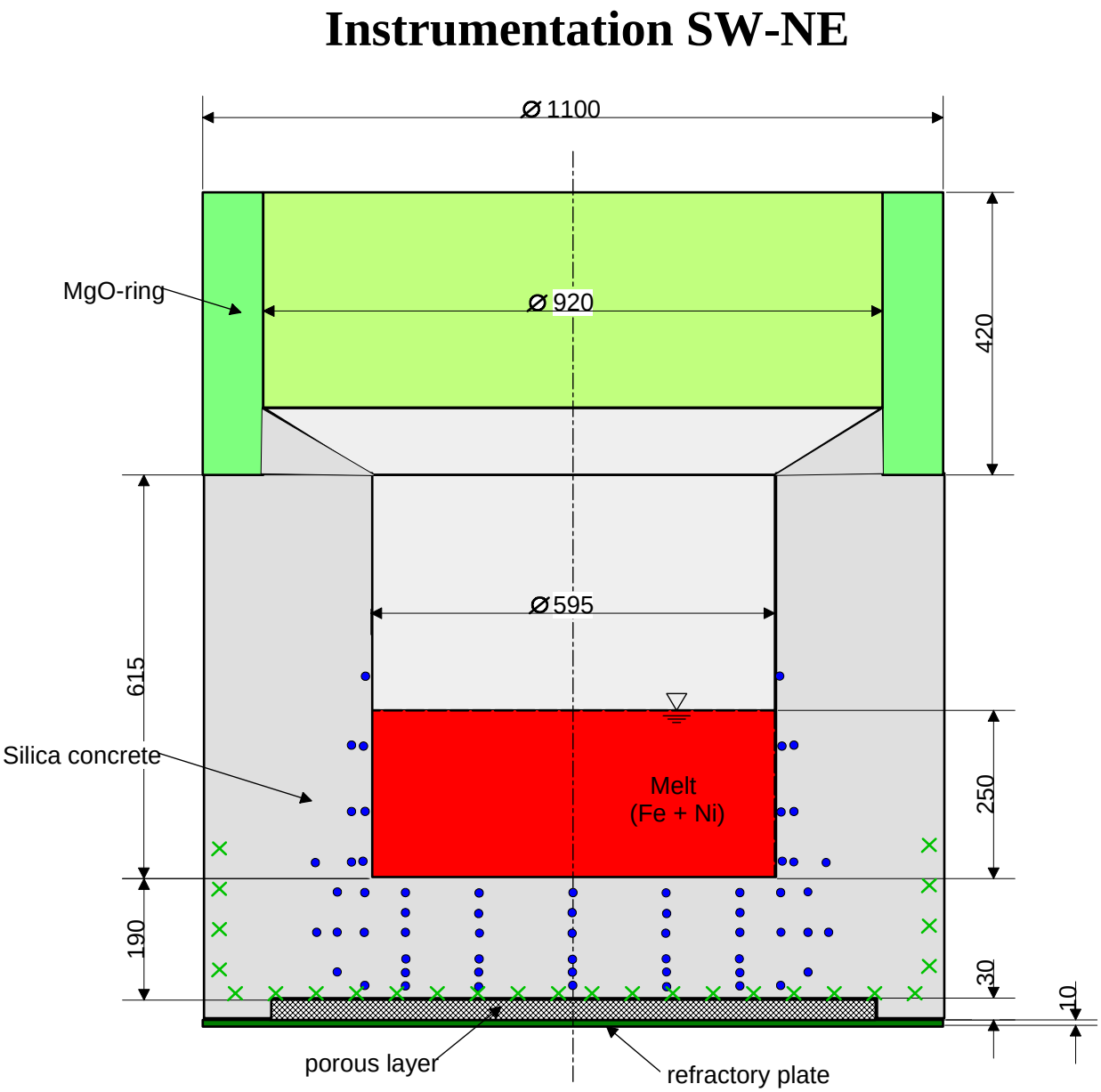

Figure 4: Thermocouple instrumentation in plane SW-NE

- 60 NiCr-Ni thermocouples

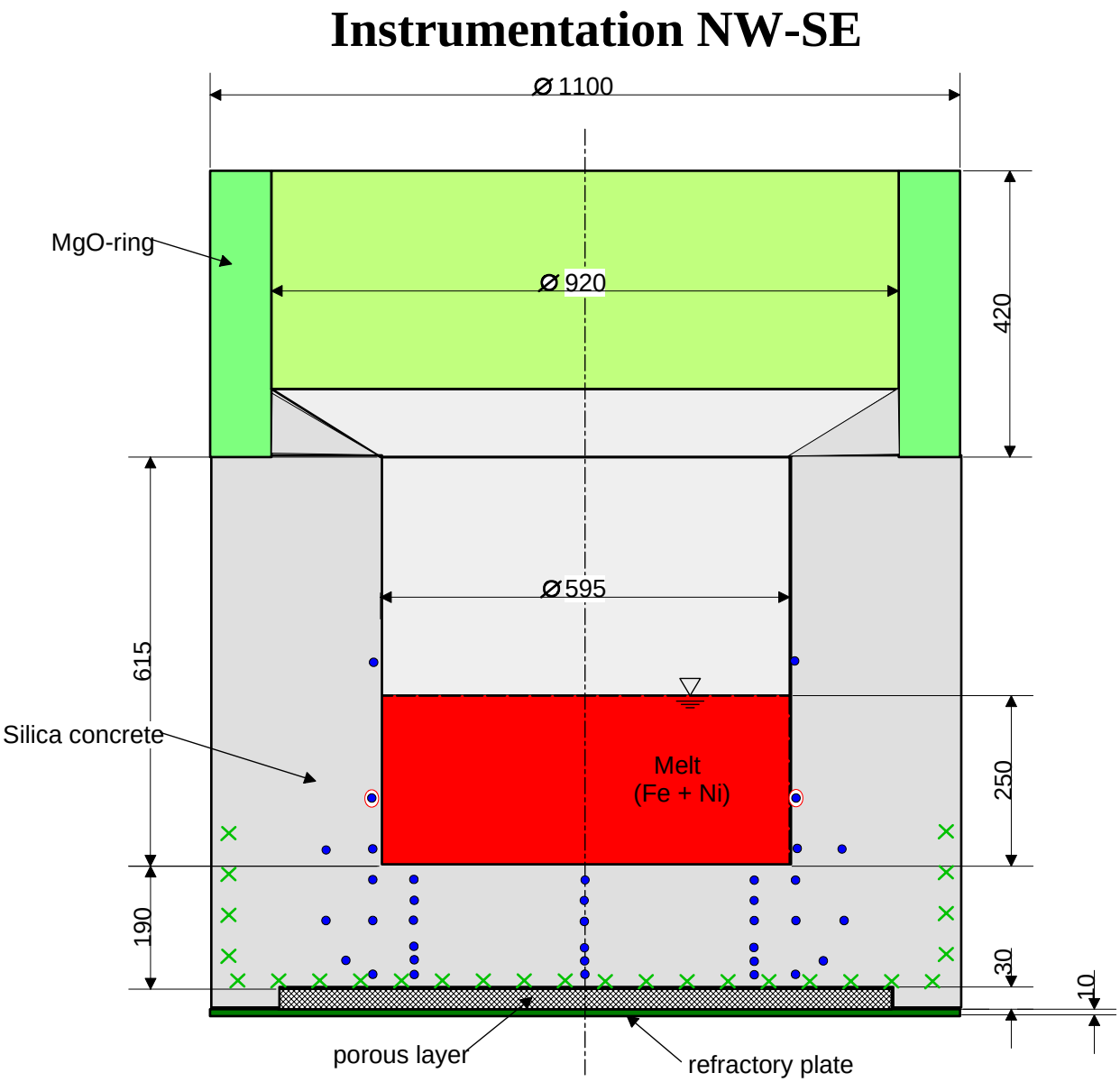

Figure 5: Thermocouple instrumentation in plane NW-SE

- 30 NiCr-Ni thermocouples (without TC on centerline)

Table 4: Position of NiCr-Ni Thermocouples in Plane SW-NE COMET-L2

Height, mm	Radius, mm							
	0	± 140	± 250	± 310	± 330	± 350	± 380	± 460
290				•				
190				•	•			
90				•	•			
15				•	•		•	
-30	•	•	•	•		•		
-60	•	•	•					
-90	•	•	•	•		•	•	
-130	•	•	•					
-150	•	•	•			•		
-170	•	•	•	•				

Total number of TC's in plane SW-NE = 60

Table 5: Position of NiCr-Ni Thermocouples in Plane NW-SE COMET-L2

Height, mm	Radius, mm							
	0	± 140	± 250	± 310	± 330	± 350	± 380	± 460
290				•				
190								
90				(•)				
15				•			•	
-30	(•)		•	•				
-60	(•)		•					
-90	(•)		•	•			•	
-	(•)		•					
-	(•)		•			•		
-	(•)		•	•				

(•) TC already listed in Table 4

(•) These 2 NiCr-Ni thermocouples use Pt-Rh compensating cables. This has no influence on the registration of the failure time

Total number of TC's in plane NW-SE = 30 (without (•))

Total number of NiCr-Ni TC's in concrete = 90

3 Experiment preparation and experimental results

3.1 Preparation of the concrete crucible

A very laborious task to prepare the test was the fabrication of the concrete crucible with the embedded instrumentation. Figure 6 shows the light guides with their black plastic sheathing, located in the lower plane of the crucible, and the thermocouples that are fixed to rods of glass for exact positioning. Figure 7 to Figure 9 show different steps to fill in the liquid concrete in the prepared mould. Figure 10 shows the final step in which the bottom porous concrete layer is prepared, during which the crucible is turned over. The curing time was more than 4 weeks so that the concrete complies with the technical specifications.

Figure 6: Instrumentation during crucible fabrication: Light guides (black sheeting) and thermocouples fixed to glass rods

Figure 7: Fabricating the bottom of the concrete crucible

Figure 8: Fabricating the concrete crucible

Figure 9: Fabrication of the cylinder wall of the concrete

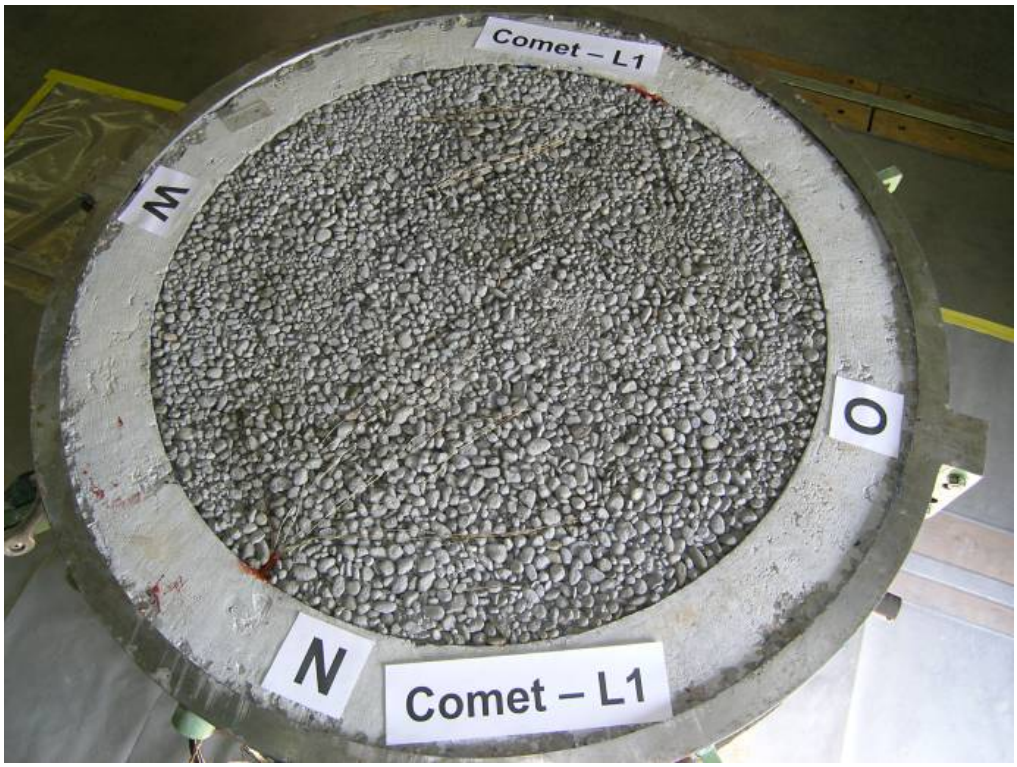

Figure 10: The 4 cm thick porous concrete layer under the crucible (upside down)

3.2 Planned performance

A brief overview of the planned test is given below.

After preparation of the melt through thermite ignition in the external thermite vessel, the test starts with pouring the melt into the crucible, with a typical duration of 40 s. Induction heating is operating at the maximum induction voltage of 2.6 kV, according to the specified net heating power of 250 kW to the melt. This heating power should be maintained between 220 and 270 kW until the declared end the first test phase.

During **Phase 1** of the test, we allow dry concrete erosion into the downward direction until approximately 130 mm are eroded, corresponding to the 4th level of thermocouples in the bottom plate. If however during the course of phase 1 the input power is not sufficient to suppress growth of a stable bottom crust, the net power to the melt may be increased to a power level up to 300 kW, if the induction voltage remains below 2.6 kV.

When the thermocouples at the 130 mm level indicate arrival of the melt front, **Phase 2** of the test is started by decrease of the net input power to about 200 kW (to be maintained between 220 and 180 kW). Duration of this phase is limited by 40 mm downward erosion until the melt is detected at the 6th thermocouple level at –170 mm. The expected time for phase 1 is 25 minutes, for phase 2 10 minutes.

After end of heating and after a few minutes for cool-down of the melt, flooding of the porous bottom layer and of the gap between the outer concrete crucible and the cylinder wall will be initiated. This should protect the induction heating coil from the hot (solidifying) melt. The water shall only stabilize the residual crucible, and is not expected to penetrate into the melt, so that the concrete and melt remain in the status as they were at the time when heating was stopped.

In case of detection of the melt front by the light guides heating will be switch off automatically or by the operator.

Two days after the test, careful disassembly of the test rig did start. Sectioning of the solidified melt in the residual crucible will be performed to complete post test analysis.

Table 6: Planned conduct of COMET-L2

Time [s]	Event
- 600	Argon cover gas flow 50 m^3/h
- 140	Start of induction heating system with 2,0 kV
-90	Ignition of thermite
0	Start of melt pour, 460 kg steel melt
30	End of pouring
60	Hood closed
> 120	Net heating power between 220 and 270 kW
300	Start of slow erosion, reduction of voltage to keep 250 kW power
1500	130 mm axial erosion, reduction of voltage to obtain 200 kW power – Start of phase 2
2100	170 mm axial erosion and end of induction heating, After some cooling slow quench from bottom and sidewalls to protect the induction system
Post test	1800 s – 3600 s additional cooling with water from bottom and sides ~ 40 h cooling down of the crucible

3.3 Course of the test

The test COMET-L2 was conducted on February 5, 2005, starting at 11:00 local time. The experimental team arrived two hours in advance at the site to start with the preparations of the test. At 10:25 the experimental hall had to be evacuated.

The control of the experiment took place from the control room with all equipment for online measurements.

After careful preparation of the test and check of all measurement and control systems, inertisation of the test rig by argon cover gas flow started 30 min before pour of the melt. The induction heating system was started and operated under the nominated voltage. The mixed and pre-heated thermite powder was ignited in the external vessel 90 seconds before the pouring. The thermite reaction was completed after 33 seconds. After further 57 s to allow separation of the metal and the oxide phases, the major part of the melt was discharged into the concrete vessel (465 kg) as shown in Figure 11. This defines time t = 0, corresponding to 11:00 local time depicted in some of the video registrations. Release of the melt to the

concrete cavity took 18 s. The melt consisted of 430 kg steel and 35 kg oxide. The residual oxide melt mass was poured into the slag wagon.

The initial temperature of the melt as measured in the spout was 1760°C (see Fig. 12).

Just at the beginning of the test the gas analysis system failed, therefore no gas data were available and no chemical gas analysis could be performed.

The most significant events during the test sequence are listed in Table 7.

Table 7: Sequence of COMET-L2 as observed during the test and from video-film

Hour	Time[s]	Event
10:57:20	-160	Induction system started, voltage 2.0 kV
10:58:30	-90	Ignition of thermite, completion of thermite burn after 33 s
10:59:40	-20	Operator increases induction voltage to 2.6 kV as specified
11:00:00	0	After count-down according to plan, start of melt pour. Full melt jet released, hits inner wall of MgO tube and rim of upper crucible, and rapidly flows to bottom of crucible. Initial temperature of melt ~1760 ±20 °C. Gas measurement system fails: Scan function not operating. No chemical gas composition measured throughout the test.
11:00:18	18	Pour of 465 kg melt (~430 kg metal melt + 35 kg oxide melt) completed. Residual oxide melt poured into slag wagon.
11.00:28	28	Spout to position 2
11:00:31	31	Command to close crucible hood. Melt has very low viscosity. Intense agitation of melt surface. Some melt splashed to upper crucible rim and to inner MgO tube, from which the melt flows back to the central crucible. (Remaining melt film at the wall forms a nearly closed, solid steel sheet, as recognized by post test analysis). No difference observable between metal and oxide melt phases – phases might be mixed. Slight aerosols in crucible until 90 s.
11:00:50	50	160 kW net power, hood of crucible locked
11:01:00	60	intense melt agitation ongoing with low viscosity
11:01:30	90	189/1250 kW net/total induction heating power at 2.61 kV lower than expected. Inductor voltage remains unchanged until 570 s, as no further voltage increase possible. Future power increase is due to increase of heating efficiency by smaller distance to the induction coil. Strong

		agitation of the melt equally distributed over melt surface, but nevertheless small splash-out of melt only. Melt surface has low viscosity, corresponding to the expected steel melt. Very clear video of the crucible, aerosols nearly zero. Small H2-flame at end of off-gas line.
11:02:20	140	170/1240 kW net/total heating power at 2.61 kV. Clear video of the crucible. Surface of melt covered by a layer of oxide melt (higher viscosity than before), may be due to ongoing concrete erosion. Intense agitation ongoing. No aerosols throughout the further test. H2 burn of off-gas ended.
11:03:00	180	189/ 1260 kW net/total heating power at 2.61 kV, strong melt agitation, viscosity of upper oxidic melt layer increased. Gas flow from the eroding concrete determines the flow pattern of the turbulent melt: Upwards at the cylinder wall, downwards in the center. Off-gas with condensing steam
11:03:20	200	Downward erosion of concrete between – 30 and –60 mm.
11:04:00	240	194/1280 kW at 2.61 kV. Oxidic melt surface more viscous strongly agitated. Off-gas has low content of condensing steam.
11:05:00	300	200/1280 kW at 2.61 kV. Gas release evenly distributed over oxidic melt surface. Some eruptions eject melt, partly metallic, to rim of concrete crucible. Low off-gas flow
11:05:30	330	Erosion approaches -60 mm, further increase of viscosity and some reduction of melt agitation.
11:06:30	390	217/1290 kW at 2.61 kV, oxide melt has higher viscosity, upper oxidic melt layer includes some bright metallic droplets, splash-out of melt reduced with exception of some more vigorous events, low condensing steam in off-gas
11:07:30	450	227/1300 kW at 2.61 kV. Gas release evenly distributed over oxidic melt surface. Gas bubble transports hot melt from the bulk to the surface. Increased steam flow at off-gas tube, no increase of gas release visible in crucible.
11:08:10	490	250/1320 kW at 2.61 kV, planned net power achieved
11:08:20	500	244/1300 kW at 2.61 kV. Power input to the melt does not show high frequency fluctuations since the early test phase. This indicates stable coupling of the metal melt to the induction field and minor metal relocation. Period of stronger melt agitation and some stronger melt eruptions. Low off-gas flow. Temperature in the lower crucible, displayed at operator’s desk, is still unchanged (at room temperature).

11:09:20	560	260 kW. Significant eruption of metal melt in south of crucible. This results in temporary increase of the heating efficiency. Start of manual reduction of induction voltage by operator.
11:09:50	590	240/1160 kW at 2.42 kV. Still some periods of higher melt eruptions. Melt approaches – 90 mm level.
11:10:55	655	Further reduction of induction voltage due to steady increase of heating efficiency. 250/1100 kW at 2.36 kV. Intense agitation ongoing. Gas flow equally distributed over melt surface. Oxide melt has higher viscosity and transports some dispersed metal droplets. Temperature in porous layer under crucible still near room temperature. Low off-gas flow.
11:11:50	710	Power reduction from 268 to 250 kW. Melt further on well agitated with some metal droplets. Melt approaches –130 mm level.
11:12:30	750	Power reduction from 268 to 250 kW/1050 kW at 2.26 kV. Oxide melt has lower viscosity with stronger agitation.
11:13:40	820	-130 mm level eroded. Start of Phase 2 of the test: Power reduction to 200 kW target value: 200/714 kW at 1.86 kV. Ejection of some metal melt.
11:14:30	870	Power reduction to 200 kW/695 kW at 1.80kV. Melt well agitated, increased viscosity of oxide, no more metal droplets visible. Low off-gas flow, -170 mm eroded as indicated by failure of BT 58
11:15:45	945	Again power reduction to 200 kW. Decision to continue heating until light guides are destroyed by melt.
11:16:10	970	205/626 kW at 1.69 kV. Melt is well agitated, oxide more viscous with some metal droplets. Air flow through porous layer under crucible still cold, indicating that melt did not yet penetrate the lower bottom.
11:16:55	1015	Heating switched-off automatically by failure of light guide CX 4. No further heating takes place, as melt reached the lower bottom. Agitation of melt by gases continues. Condensing steam in off-gas flow.
11:18:20	1100	Air flow in porous layer still cold (20°C), melt and surface still liquid, outer crucible as indicated on operator panel still at 30°C only.
11:18:40	1120	Light guide CX 4 repeats failure signal (was possibly “repaired”)
11:19:14	1154	Light guide CX 3 interrupted, both failed light guides are located in N hemisphere. Ongoing gas bubbles transport hot melt from the bulk to the surface.
11:20:50	1250	Oxide surface near cylinder wall forms dark crust, central surface still bright and liquid, and further on agitated by gas bubbles. Bulk of melt

		still at high temperatures. Low off-gas flow.
11:22:00	1320	Dark ring of crust broadening. Bright central surface of melt reduced to some 30 cm diameter
11:22:20	1340	Cooling of bottom of concrete crucible activated by supply of coolant water to N and S of the porous concrete layer under the crucible. Continuous coolant flow from 1.5 to 0.65 l/s, coolant water shows no temperature increase. Cooling does not initiate intense processes in crucible or melt. Off-gas flow with condensing steam.
11:24:00	1440	Bottom cooling ongoing with 0.62 l/s driven by 3 m water overhead.
11:24:10	1450	Surface of melt dark, only center bright and still liquid
		Tape changed
11:25:00	1500	Remaining hot spot in the center of ~10 cm dia with release of gas bubbles. Surface crust smooth and gas tight
11:26:40	1600	Bottom flooding ongoing with 0.69 l/s, central surface still bright, off-gas with condensing steam. Maximum downward erosion occurred probably in SW
11:28:50	1730	All light guides under crucible failed by contact with the hot melt/regulus
11:30:00	1800	Bottom flooding ongoing with 0.66 l/s, with minor increase of the water temperature only. No water visible in upper crucible.
11:31:00	1860	Surface of oxide covered by dark crust, some hot lines probably due to cracks indicate the hot temperatures in the bulk of the oxide melt
11:31:40	1900	Lights in crucible on, fine glass whiskers visible above the dry surface, Surface crust is convex, smooth, and closed. Steam flow in off-gas seems ongoing.
11:33:20	2000	Water inflow to porous concrete interrupted. Water level in outer annulus of the concrete crucible, which was filled with water up to 70 cm, slowly reduces to 10 cm. Existence of water in the annulus indicates cracks which allow permeation of water from the porous sublayer to the annulus.
11:34:12	2052	Water inflow to porous concrete resumed, resulting in 0.72 l/s. Only small increase of water temperature (20.4°C). Thermocouple BT 34-37 in lower crucible show ~ 70°C. Melt evidently stopped close to the porous layer, no further erosion of concrete expected.
11:37:10	2230	Water inflow to porous bottom layer is 0,69 l/s, water level in annulus 64 cm due to leakage from bottom layer. Small leakage of water from outer crucible, where instrumentation lines are introduced; this leakage

		confirms that annulus is flooded.
11:40:00	2400	some hot spots still visible through the upper oxide crust, central part of the oxide still hot, bottom cooling continued
11:45:00	2700	Direct water supply to annulus started with the goal to flood the surface of the melt by overflow from the annulus.
11:45:05	2705	Water enters surface of melt, strong foaming
11:46:10	2770	Surface of melt practically covered with foaming water in moderate pool boiling, convex crust, total water flow to bottom and annulus 1.04 l/s
11:48:00	2880	Surface of crust covered by 10 to 20 cm water layer, moderate pool boiling, steam in off-gas
11:50:00	3000	Further activities directed to cool the melt and to extract the energy, keeping the outer test rig and the induction coil sufficiently cool
11:56:40	3400	Melt flooded, total water inflow to bottom and sidewall ~0.52 l/s, minor boiling in water layer, measured water level in the annulus is 73 cm, condensing steam flow in off-gas
12:00:00	3600	Water level in crucible raised up to 10 cm below upper rim of the Mg0 ring, minor boiling, gases are released from water layer in east and to minor extend in west, temperature measured at the lower melt/concrete interface still 1200°C typical. Extraction of heat strongly limited by conduction through remaining concrete at bottom and side, and through crust at upper surface. Crucible is completely enclosed by water.
12:03:50	3830	Shower head activated to add water from the crucible hood
12:10:00	4200	Stop of flooding through shower head
12:14:00	4440	Drainage of water from the upper water layer through the melt to the porous concrete layer is not successful: No cracks in the solidifying melt or at the melt/concrete interface, which allow passage of water. Very small steam flow in the off-gas.
12:22:00	4920	Again activation of shower head
12:36:40	5800	End of experiment declared, temperatures at melt/concrete interface in lower crucible still 1000 -1100°C
		Further flooding and draining to remove the heat, crucible remains flooded for long- term heat removal over the rest of the day to extract the energy

3.4 Test results

3.4.1 Mass and temperature of the melt

As described above the mixed and pre-heated thermite powder was ignited in the external vessel 90 seconds before the pouring. The thermite reaction was completed after 33 seconds. After further 57 s to allow separation of the metal and the oxide phases, the major part of the melt (465 kg) was discharged into the concrete vessel (Figure 11). Release of the melt to the concrete cavity took 18 s. The melt consisted of 430 kg steel and 35 kg oxide. The residual oxide melt mass was poured into the slag wagon.

The initial temperature of the melt as measured in the spout was 1760°C (see Fig. 12).

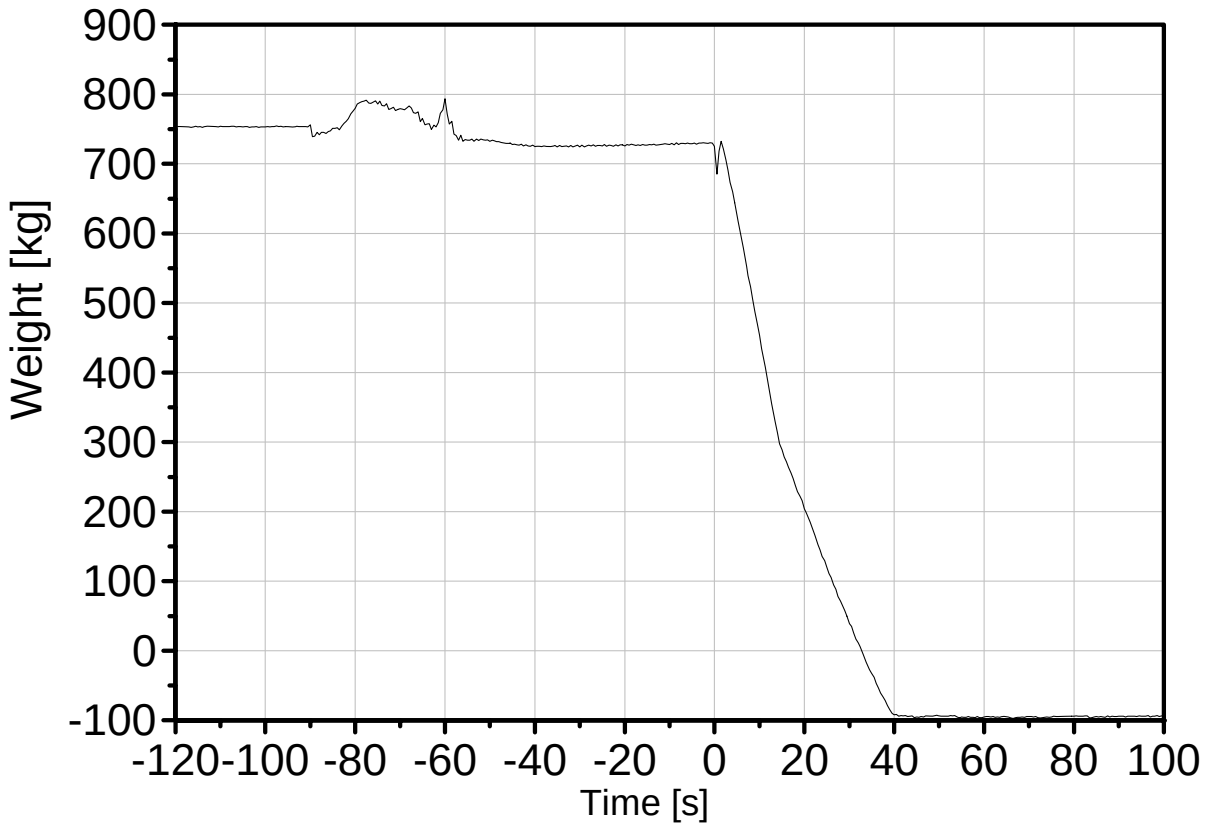

Figure 11: Melt release from the thermite vessel

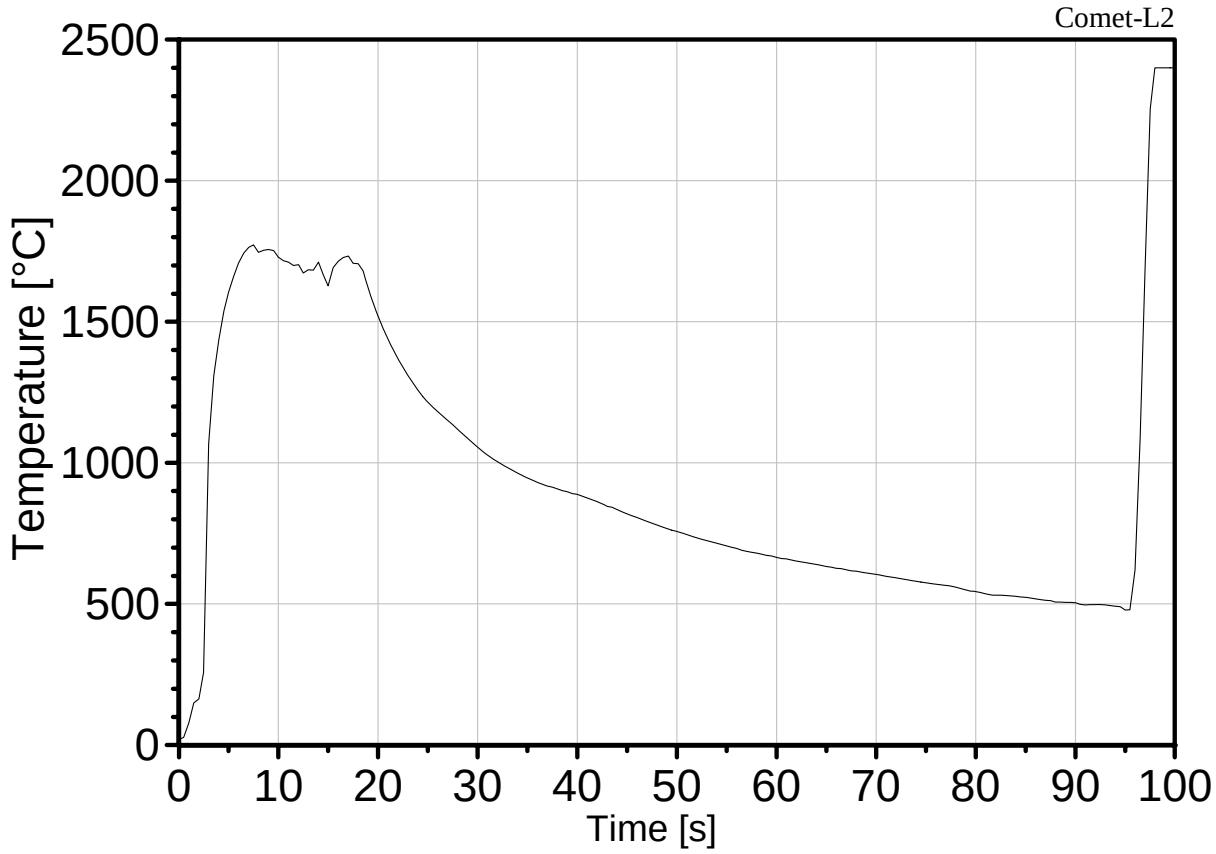

Figure 12: Melt temperature in the spout

As in the COMET-L1 experiment, an infrared video camera was installed on top of the hood of the crucible at a distance of ~2.5 m from the melt surface. This camera operates in the near infrared spectrum from 3.4 to 5.0 μm to produce a video film and, every 15 s, up to 240 high precision thermal images of the melt surface during 60 min. The camera utilizes a 3.9 micron flame suppression filter and is placed behind a 3 mm thick sapphire window which has a transmission coefficient of ~0.9 at the considered wavelength.

In experiment COMET-L2 only the metal part of the thermite melt (Fe + Ni) was poured into the crucible; therefore the following assumptions have been made to determine the temperature of the metal melt jet. Different estimates for the spectral emittance of the molten iron performed in the steel industry come up with an emissivity value of 0.2-0.5 depending on temperature and wavelength. Taking into account the conditions of the COMET-L2 test and the operating spectrum of the infrared camera, a value of 0.3 has been chosen for the current analysis.

Two thermal images of the iron melt stream have been taken 11 and 15 seconds after the start of the pouring process. These thermal images, corresponding visual pictures, and temperature histograms of the melt pouring process in the COMET-L2 test are shown in Figure 13.

Thermographic analysis shows that the estimated temperatures of the melt stream are within a range of 1600-1850 °C with a distinct maximum at 1700-1750 °C. These estimates are in fairly good agreement with the 1750 °C measured by a W/Re thermocouple in the spout (compare Figure 12). The brighter areas in the thermograms are due the oxide film on the surface of the iron melt pool, that forms immediately upon onset of the concrete erosion. This higher emissivity must be accounted for when evaluating the temperature of the pool surface.

In the beginning of the experiment, the oxide melt mainly consists of iron oxide. With increasing concrete erosion, concrete decomposition products, in particular silicates, are admixed into the top oxide layer. Therefore the oxide melt composition and, consequently, the emissivity of the melt constantly changes throughout the experiment, making it impossible to evaluate the melt temperature using a constant value for the emissivity coefficient.

Assuming the associated emissivities for the initial melt as 0.7 for pure iron oxide and as 0.3 for pure SiO_2, maximum temperatures of the melt surface, that are close to the melt bulk temperature, were determined for later phases of the experiment. The two temperatures of the melt shown in Figure 14 give the boundaries for the true surface temperature. During the first minutes of the test the melt temperature is certainly close to the red line dominated by the emissivity of iron oxide. At the end of the experiment the melt temperature would be closer to the blue line (temperature of pure SiO_2), that is near 1000 °C after heating was terminated at 1015 s.

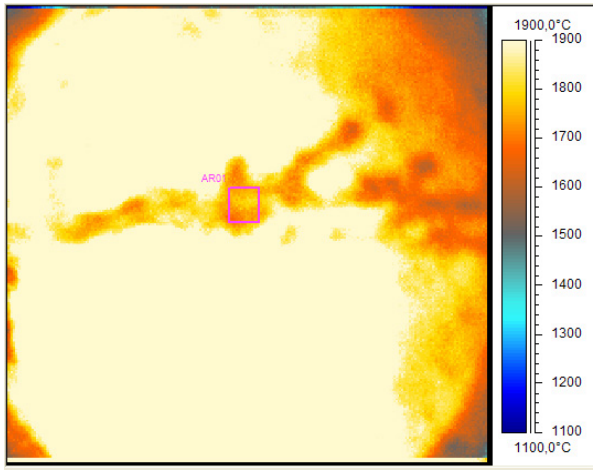

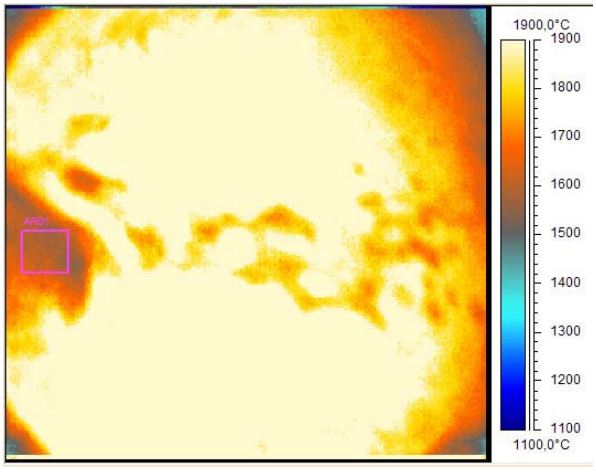

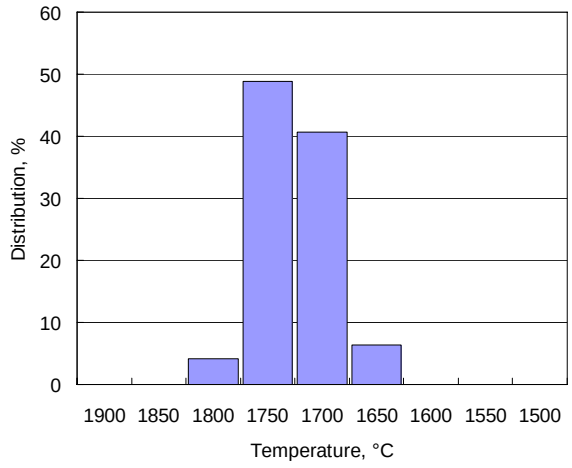

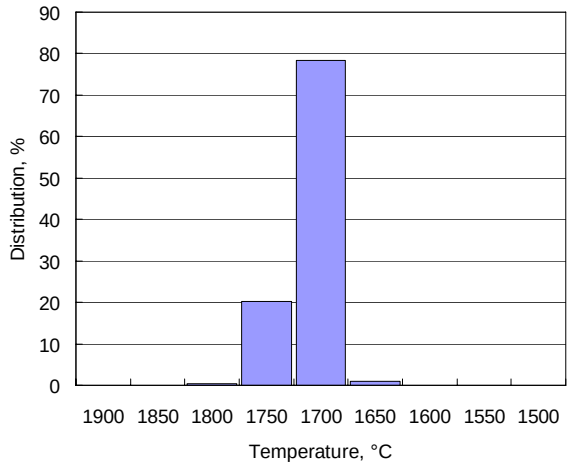

a) b)

Figure 13: Iron melt stream a) 11 s and b) 15 s after the onset of the melt pouring. Visual pictures, corresponding thermograms, and temperature distribution.

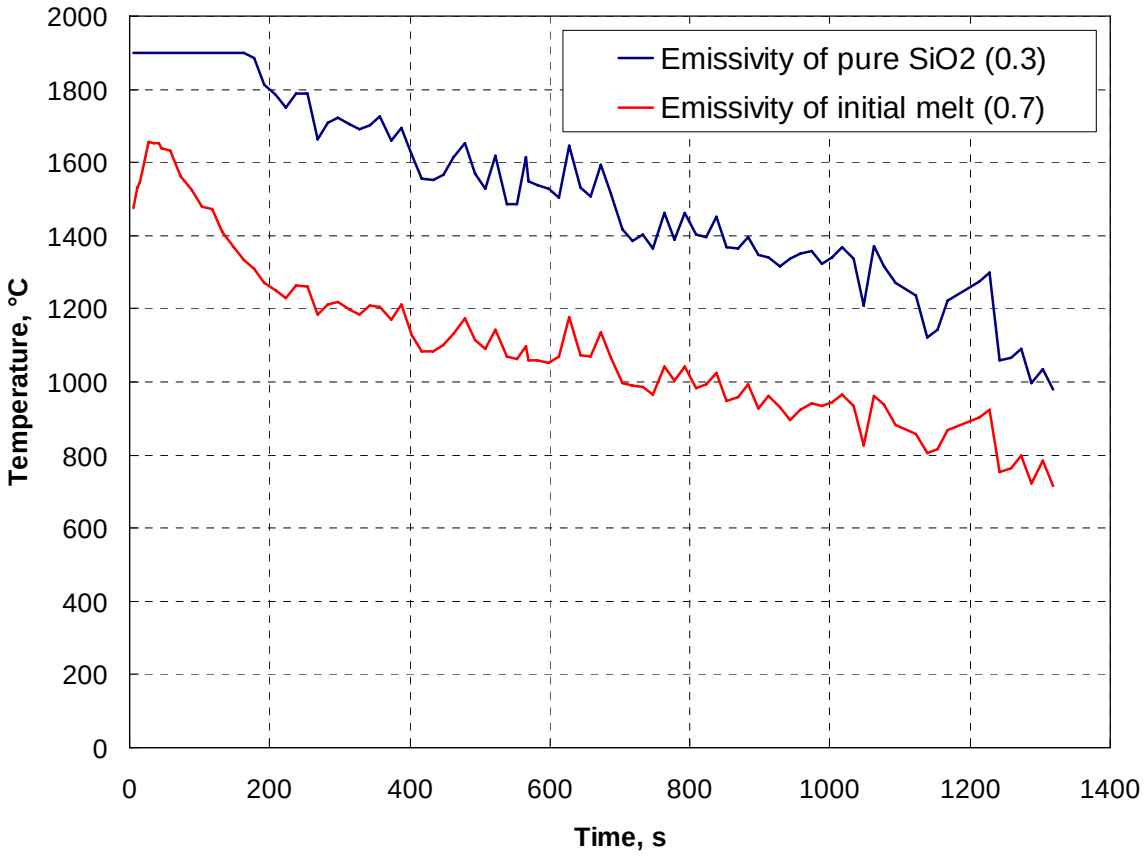

Figure 14: Evolution of the maximum measured temperatures of the melt surface assuming the emissivity is 0.7 (lower curve - initial oxide) and 0.3 (upper curve - late oxide)

3.4.2 Decay heat simulation and melt behaviour

Operation of the induction system to simulate the internal decay heat in the melt was started some 2 minutes before the melt was poured into the crucible. The voltage of the induction coil was controlled by the operator throughout the heating period, to achieve the net power input to the melt according to the test plan. Online measurements of the net power and of the total power gave the necessary information to the operator.

Figure 15 and Figure 16 show the characteristics of decay heat simulation by induction heating. Besides the important information on power input and induction voltage, the efficiency of heating and the power fluctuations allow qualitative estimates on the status of the steel melt, as the geometry of the metal influences the electromagnetic coupling to the induction field.

The operator controls the induction voltage to achieve the desired net heating power.
The initial net power input was 160 kW, and did increase up to 189 kW for 2.61 kV at 90 s. This was lower than expected. The inductor voltage remained unchanged until 570 s because no further voltage increase was possible. The increase of heating efficiency due to the smaller distance to the induction coil generates a further power increase. The net induction power increased to 200 kW at 300 s, to 227 kW at 450 s and finally to 260 kW at 560 s. At this time manual reduction of induction voltage started. As result the net power of 250 kW for 2.36 kV at 655 s was achieved, following voltage reductions kept this value during the next 167 s. At 820 s phase 2 of the test did begin designed for a target value of 200 kW. Caused by further voltage reduction (up to 1.69 kV) the target value was kept until 1015 s when the heating system was switched off automatically due to failure of a light guide.

Three major peaks did occur: at the beginning up to 270 kW, at 560 s up to 450 kW and at 790 s up to 360 kW. The peaks correlate with events in the melt. At 560 s a significant eruption of metal melt in the south of the crucible took place (Fig. 19) causing a temporary increase of heating efficiency. At 750 s the oxide melt had a lower viscosity than before resulting in an additional eruption of melt at 790 s (Fig.20). In between the peaks there were no major fluctuations due to the high viscosity of the melt.

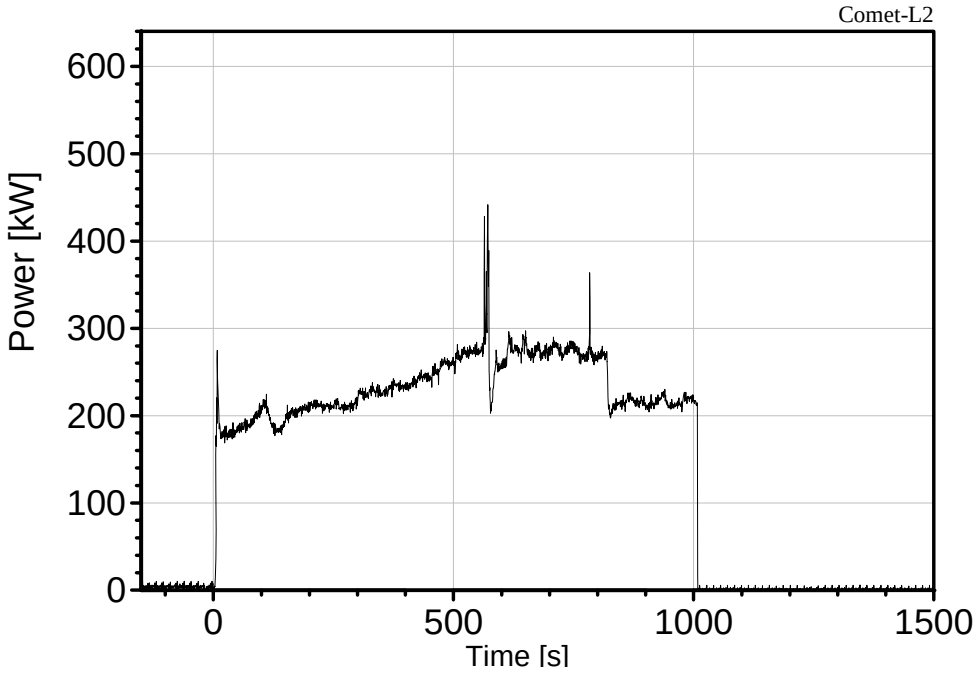

Figure 15: Net heating power in the melt

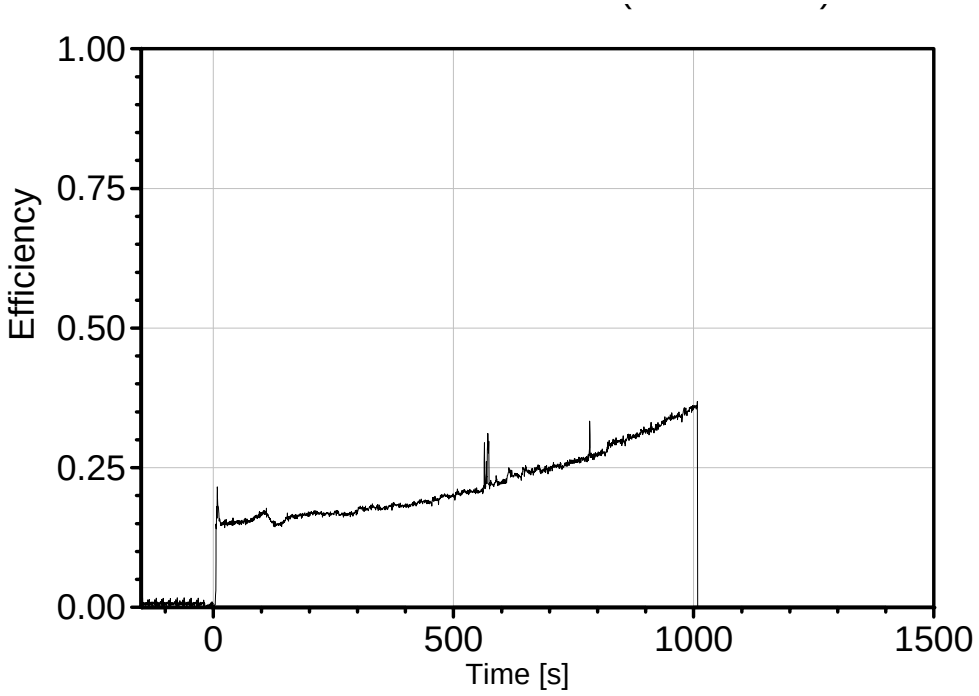

Figure 16: Efficiency of the induction heating, referred to the gross heating power

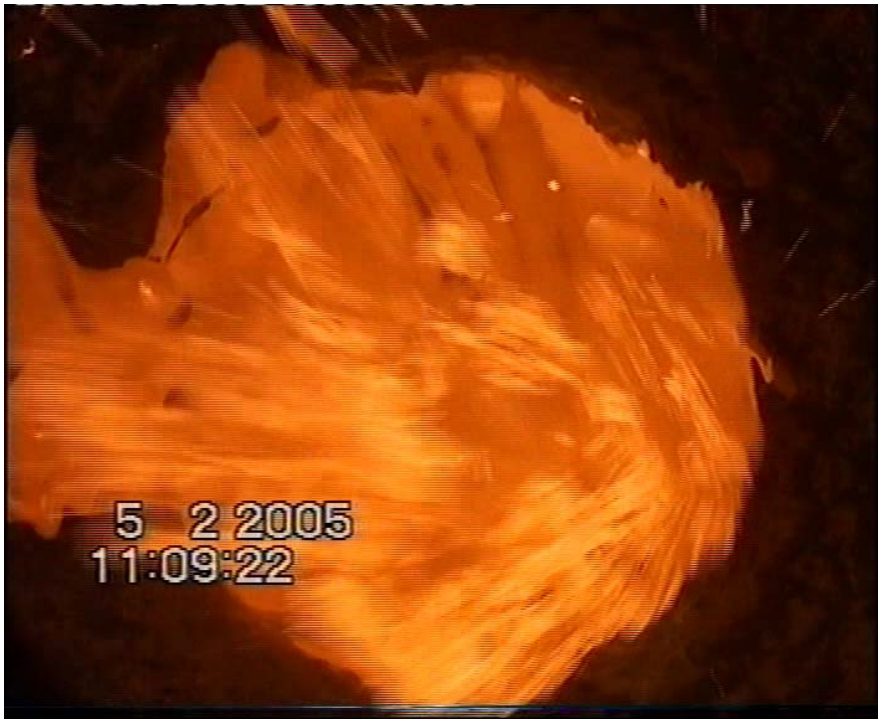

Figure 17: Melt eruption at 562 s

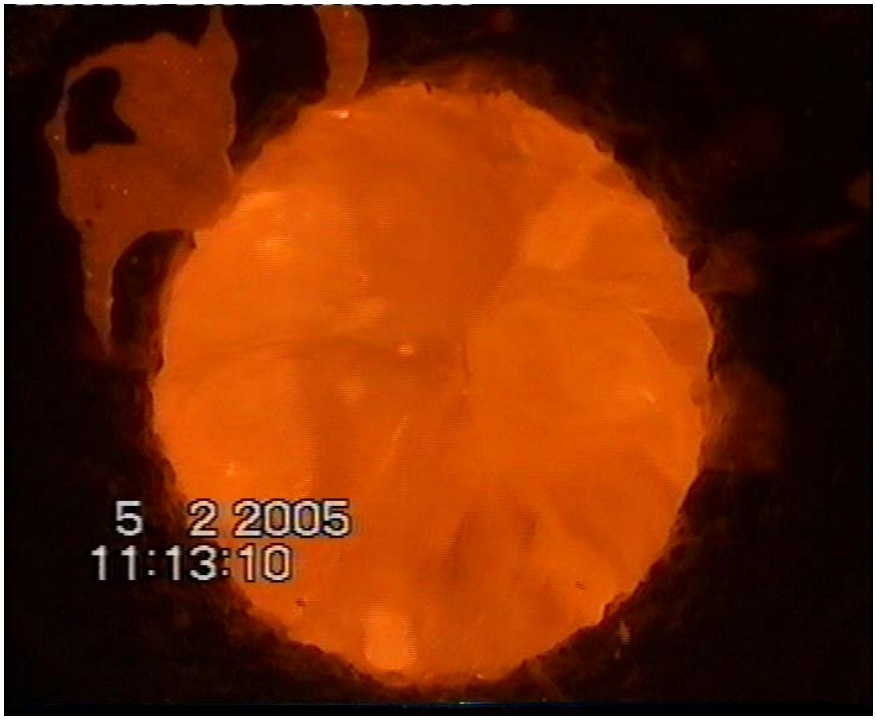

Figure 18: Melt eruption at 790 s

3.4.3 Concrete erosion and cavity shape

For a detailed analysis of concrete erosion rates and cavity shape, the failure times of thermocouples in the concrete cavity are evaluated. The thermocouples are positioned in two separate planes, namely SW – NE and SE – NW. **Table 11** in Appendix B lists all signals that are registered on the MICROLINK data acquisition system.

Figure 3 and Figure 4 contain the positions of the NiCr-Ni thermocouples. Thermocouples are located at following levels (mm): 290, 190, 90, 15, -30, -60, -90, -130, -150, -170.
In radial direction, the thermocouples are positioned at the following radii: 0 mm (centre line); 140 mm , 250 mm, 310 mm, 330 mm, 350 mm; 380 mm; and 460 mm.
Table 8 contains the true position of the failed thermocouples.

Table 8: True position of the failed TCs

contour of erosion front,
true positions of the failed TCs

plane SE-NW		x-values	y-values
horizontal	t8SE	-297,5	290
	t6SE	-310	90
	t5SE	-310	15
vertical	t4SE	-310	-30
	t3SE	-250	-60
	t1CL	0	-150
	t3NW	250	-60
	t4NW	310	0
horizontal	t5NW	310	15
	t6NW	310	90
	t8NW	310	290

plane SW-NE		x-values	y-values
horizontal	t8SW	-297,5	290
	t7SW	-297,5	190
	t6SW	-330	90
	t5SW	-330	15
vertical	t4SW	-310	0
	t3SW	-250	-90
	t2SW	-140	-170
	t1CL	0	-150
	t2NE	140	-90
	t3NE	250	-60
	t4NE	310	0
horizontal	t5NE	330	15
	t6NE	330	90
	t7NE	310	190
	t8NE	297,5	290

In the next two Tables (Table 9 and Table 10) the estimated minimum and maximum contour of the erosion front is given.

Table 9: Estimated minimum contour of the erosion front, from the behaviour of the adjacent TCs

estimated minimum contour of the erosion front, from the behaviour of the adjacent TCs

plane SE-NW		x-values	y-values
horizontal	t8SE	-297,5	290
	t6SE	-312,5	90
	t5SE	-322,5	15
vertical	t4SE	-310	-40
	t3SE	-250	-100
	t1CL	0	-150
	t3NW	250	-70
	t4NW	310	-10
horizontal	t5NW	317,5	15
	t6NW	317,5	90
	t8NW	312,5	290

plane SW-NE		x-values	y-values
horizontal	t8SW	-299,5	290
	t7SW	-302,5	190
	t6SW	-357,5	90
	t5SW	-337,5	15
vertical	t4SW	-310	-15
	t3SW	-250	-110
	t2SW	-140	-180
	t1CL	0	-150
	t2NE	140	-110
	t3NE	250	-70
	t4NE	310	-25
horizontal	t5NE	337,5	15
	t6NE	347,5	90
	t7NE	312,5	190
	t8NE	299,5	290

Table 10: Estimated maximum contour of the erosion front, from the behaviour of the adjacent TCs

estimated maximum contour of the erosion front, from the behaviour of the adjacent TCs

plane SE-NW		x-values	y-values
horizontal	t8SE	-307,5	290
	t6SE	-317,5	90
	t5SE	-342,5	15
vertical	t4SE	-310	-60
	t3SE	-250	-120
	t1CL	0	-160
	t3NW	250	-80
	t4NW	310	-25
horizontal	t5NW	337,5	15
	t6NW	327,5	90
	t8NW	327,5	290

plane SW-NE		x-values	y-values
horizontal	t8SW	-305,5	290
	t7SW	-307,5	190
	t6SW	-377,5	90
	t5SW	-357,5	15
vertical	t4SW	-310	-25
	t3SW	-250	-115
	t2SW	-140	-190
	t1CL	0	-160
	t2NE	140	-130
	t3NE	250	-80
	t4NE	310	-70
horizontal	t5NE	357,5	15
	t6NE	377,5	90
	t7NE	322,5	190
	t8NE	305,5	290

The actual erosion front is defined by failure of the thermocouples (the complete signals are given in Appendix C, Figure 29 to Figure 42). Thermocouples with incorrect signals are neglected. Thermocouple BT 75, NiCr/Ni (310, 45, 100) Log “Kanal 81” was defect, this Channel was taken for IR1 (Temp. IR-Objektiv).

Based on the estimated contour of the erosion front a probable final cavity shape is shown for each plane in Figure 19 and Figure 20.

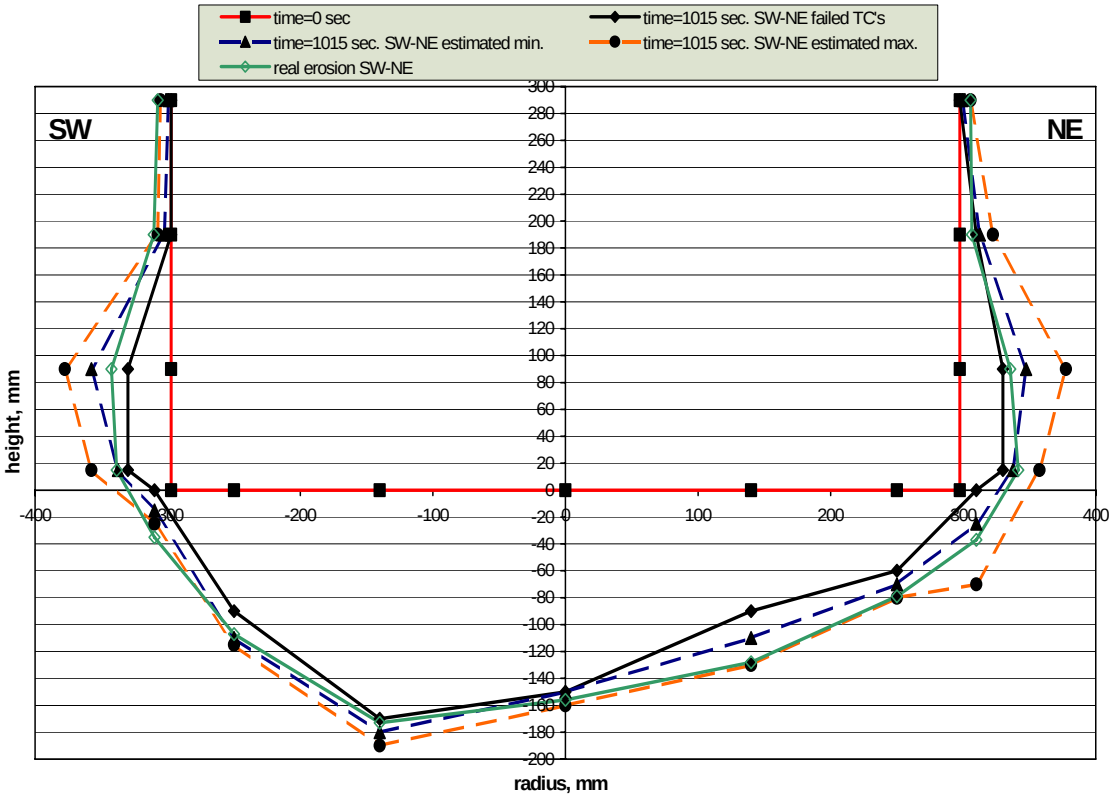

Figure 19: Initial and final cavity shape in the SW – NE plane

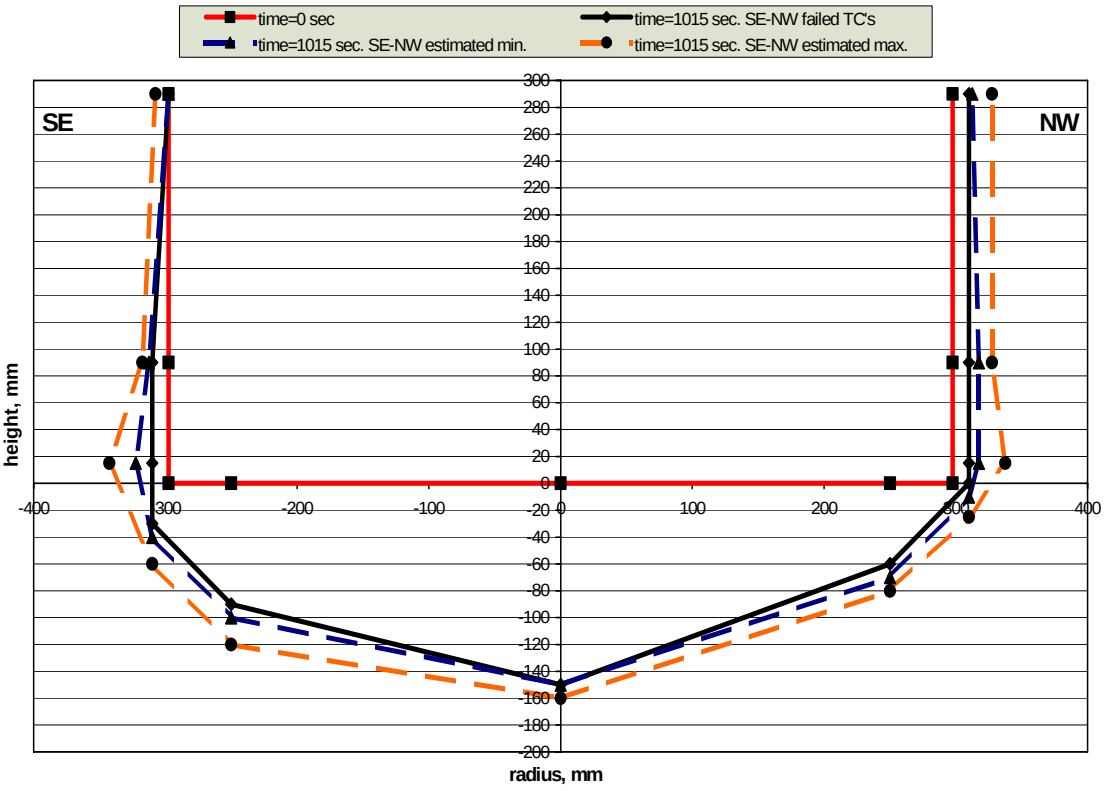

Figure 20: Initial and final cavity shape in the SE – NW plane.

Concrete erosion due to the metal melt is shown in Fig.23. The solid lines are derived from thermocouples staggered in the vertical direction, the dashed lines in the lateral direction. Downward erosion stopped between the -90 and –170 mm instrumentation plane. Maximum radial erosion is about 30 mm.

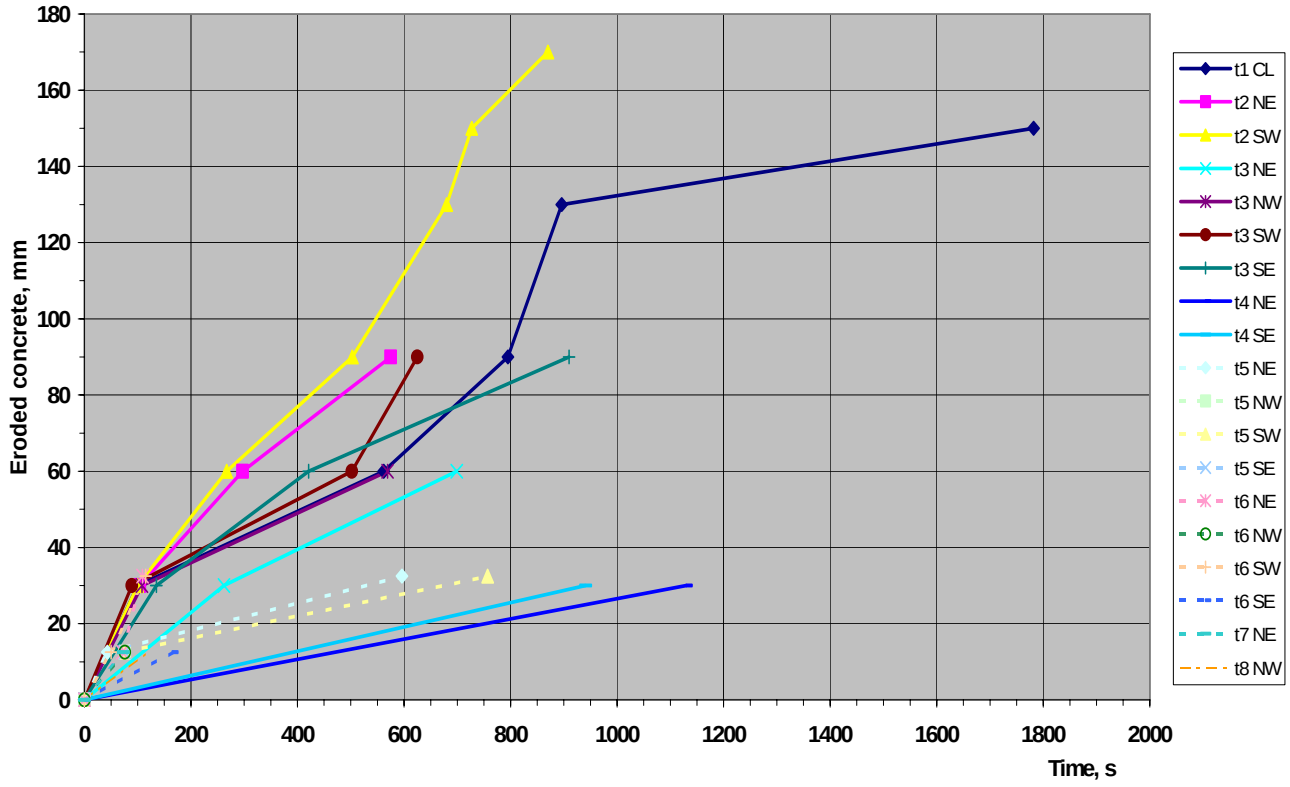

Figure 21: Concrete erosion due to the metal melt. Axial (solid lines), radial (dotted lines)

3.4.4 Gas release

Due to the fact that from the beginning of the experiment the gas measurement system failed no data about the released gas is available.

3.4.5 Long-term melt behaviour and consequences of flooding

After the heating switched off automatically (1015 s) because the light guide CX4 failed the melt stays still active by continuing gas release. During the next 200 s ongoing gas bubbles transport hot melt from the bulk to the surface. Then at 1250 s an oxide surface near cylinder wall forms a dark crust. The central surface is bright and liquid. The bulk of the melt has still a high temperature. Consequently from the outer melt region more and more oxide forms a ring of crust. Cooling of bottom of concrete crucible (1340 s) causes no intense processes in the crucible or melt. 160 s later there is only a hot spot in the center left (see Figure 22). But there

is ongoing activity in the melt (see Figure 23). 1860 s after start of the test the surface of oxide is covered by a dark crust, some hot lines indicate the still high temperature in the melt beneath. When the supplied water overflows the surface of the melt strong foaming occurs. Finally the water level was raised up to 10 cm below the upper rim of the MgO ring. Extraction of heat is strongly limited by conduction through remaining concrete at bottom and sides, and through crust at upper surface. Now the crucible is completely surrounded by water.

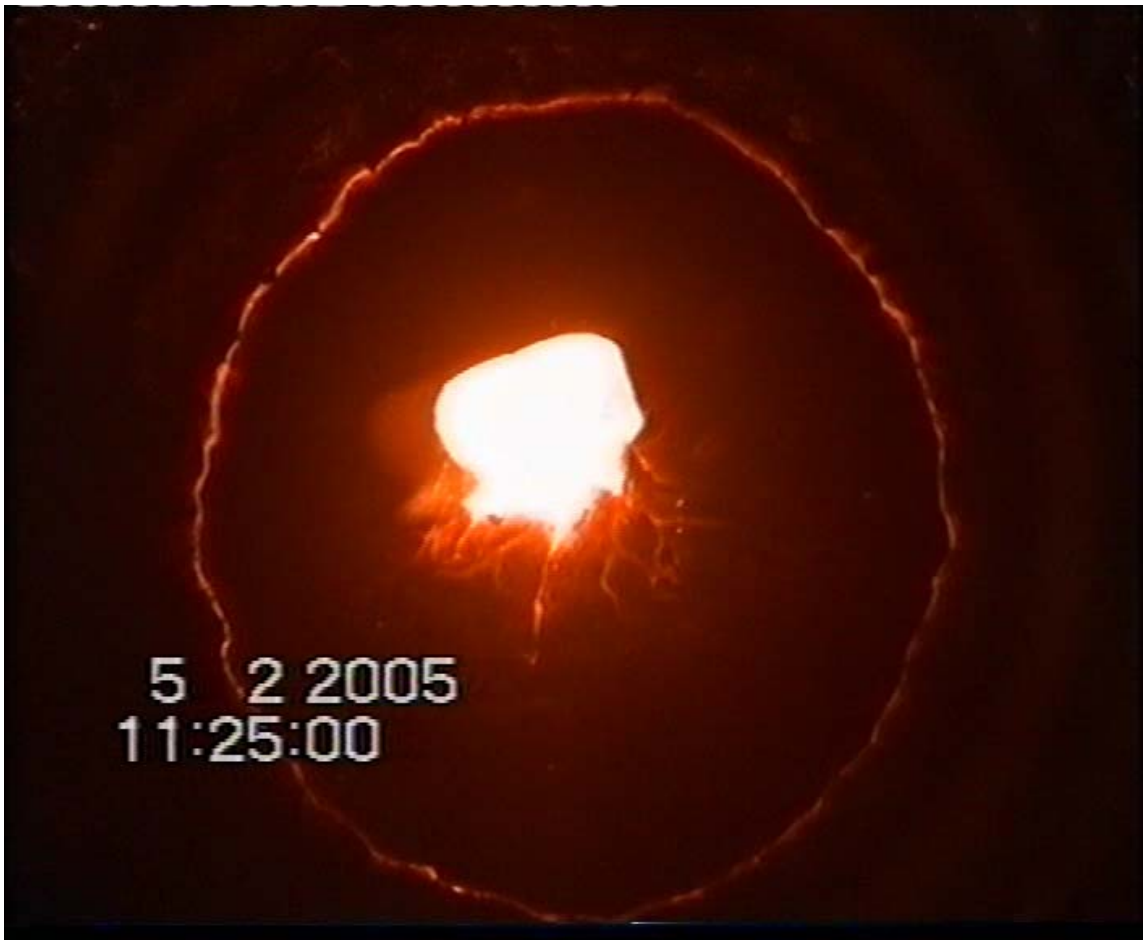

Figure 22: Oxide crust established

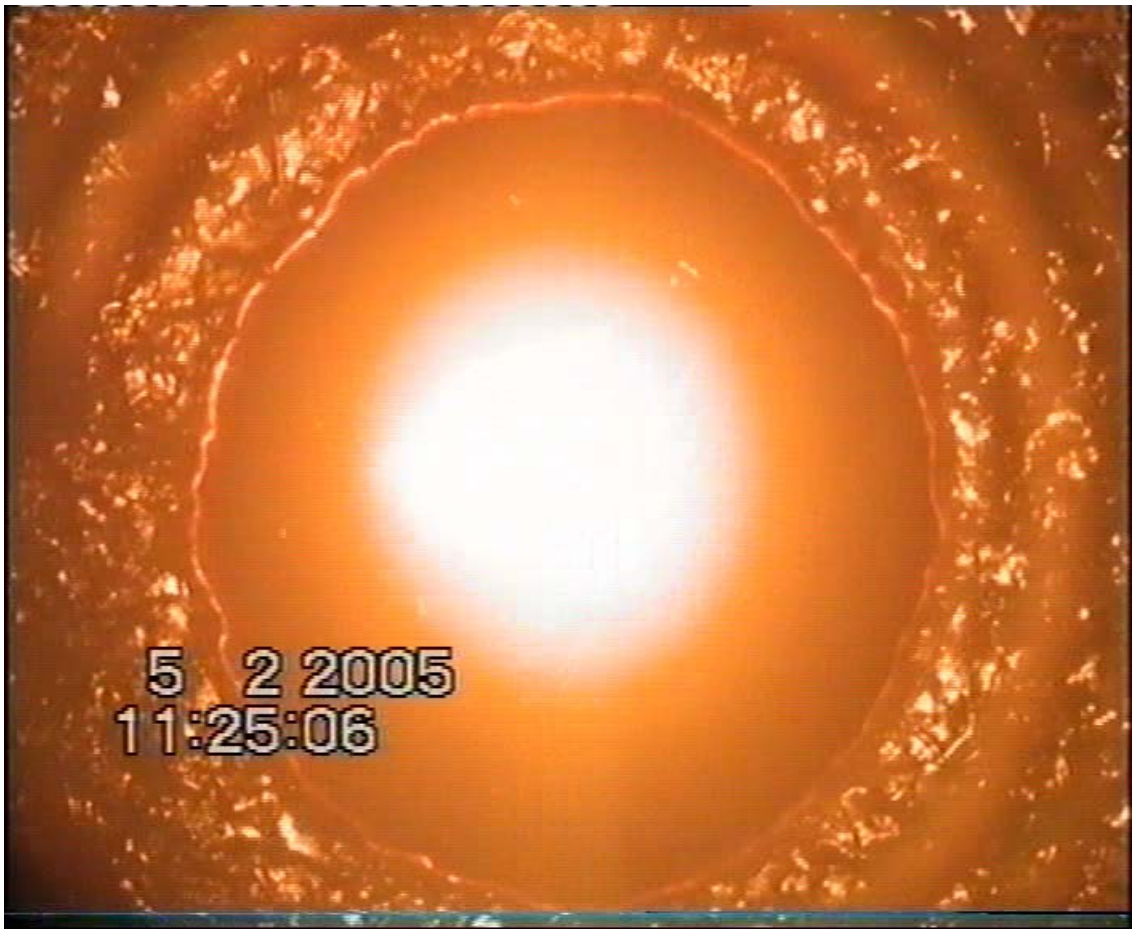

Figure 23: Ongoing activity in the melt

3.5 Post test analyses

Two days after the test, disassembly of the facility was started to document the status of the cavity and the debris configuration. A first view from above into the open crucible enclosed by the outer protection tube is shown in Figure 24 and Figure 25.

Figure 24: View from above into the open facility after the experiment

Figure 25: Closer view from above into the open facility after the experiment (without debris)

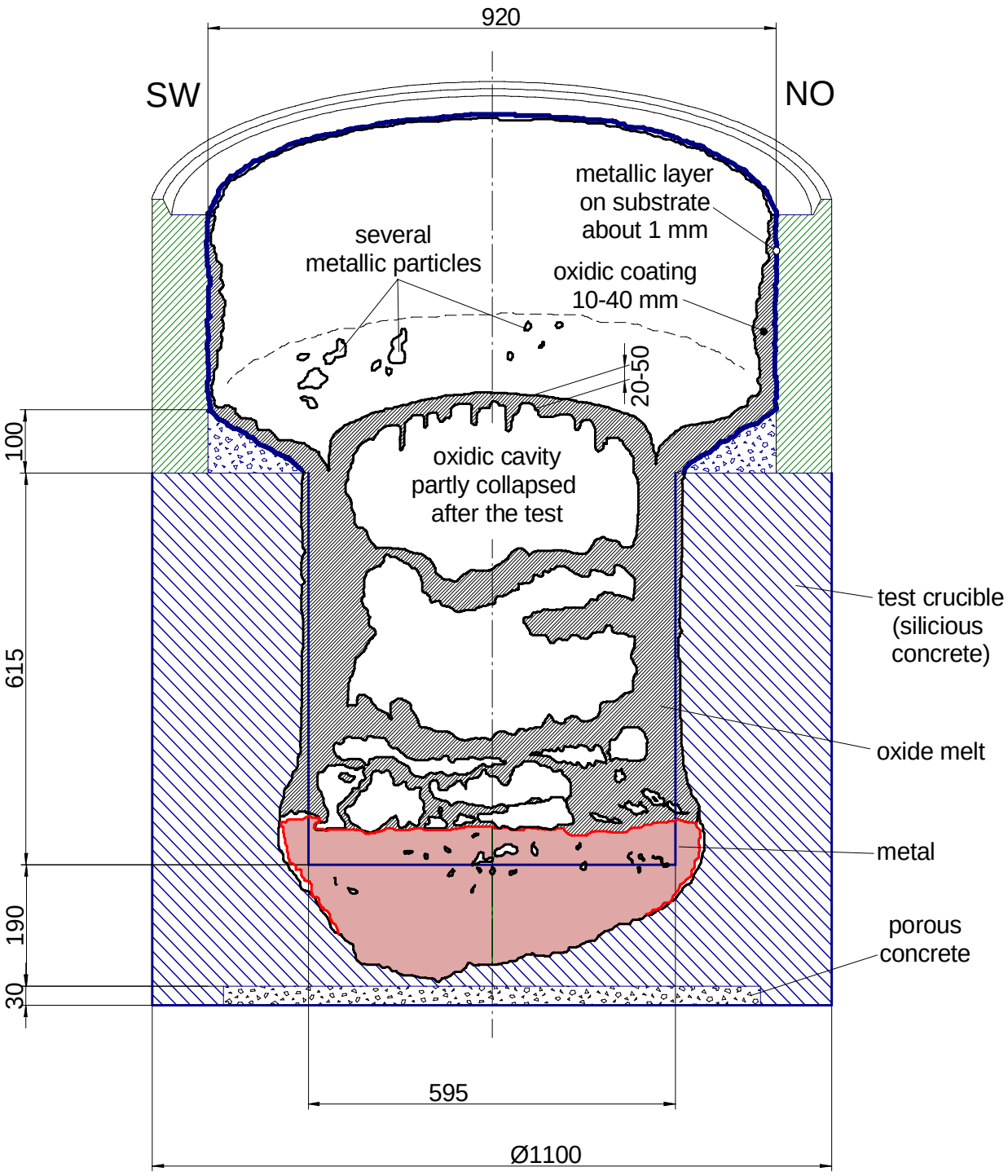

Figure 26: Contour of the melt after the test

The artist's view of the cross section of the crucible, represented in Figure 26, shows the different crusts and their structure.

In the following a description of the melt surface in the crucible is given:

- The whole MgO wall is covered by a layer of about 1 mm thick Fe. This layer was established during the first 2 minutes.
- The Fe-layer at the MgO ring is covered by oxidic melt which was generated in a later phase. In the upper part of the MgO ring the thickness of the oxidic layer is about 10 mm. In the middle part thickness of the layer is increasing up to approximately 40 mm and finally becomes thinner in the lower part.
- At the sloping part of the crucible the oxide layer is somewhat thicker.
- On the surface of the sloping part several pieces of Fe were detected. These pieces were generated during the eruption with the timestamp 9:20. Tiny droplets of Fe could be found inside the MgO ring.
- At the end of the experiment a cavity was established in the centre of the crucible with 450 mm diameter and approximately 250 mm height. The dome collapsed due to residual stress and shrinking during cooling period. The fragments are 10-50 mm thick consisting of pure oxide with small pores. The generation of the cavity started with water cooling resulting in a stable crust and release of gas bubbles from the melt.
- The bottom of the cavity consists of several bumps with a diameter between 8 and 10 cm which were generated by melt flowing through the already established crust. A small channel was found in which lava flew from the centre to the eastern rim of the crust.

Figure 27: Eroded concrete crucible sectioned in direction NE-SW

Figure 28: Eroded concrete crucible sectioned in direction SW-NE

The crucible was sectioned after the test along the main instrumentation plane SW-NE (Figure 27 and Figure 28). The lower cavity is filled with the solidified iron melt, overlaid by oxide. The yellow line marks the original geometry of the crucible and shows the erosion.

The oxide melt contains a significant amount of unmelted silica gavels which is the consequence of low heat fluxes to the concrete surface. The heated concrete loses its mechanical strength, and the aggregates may be transferred into the melt before being melted. This may result in different heat flux distribution and erosion resulting from the lower „melting“ enthalpy of concrete, and bulk cooling of the melt by aggregates.

The cavity erosion by the oxide melt is virtually zero in the upper cavity. The lower 30 cm of the sidewalls show a more pronounced radial erosion, maximum erosion about 3 cm, which is predominantly due to the attack of the metal melt. In contrast, downward erosion by the metal melt extends to some 17 cm with the maximum near the 10 cm radius. Although the uneven downward melt front is partly determined due to the inhomogeneous decay heat distribution. The more pronounced downward erosion seems to be imminent to the erosion by the metal melt for low heat fluxes. This is in agreement with the former BETA experiments V 3.1 to 3.3 [8] at low induction power. Induction heating was performed with a cylindrical induction coil with the result that a nonhomogenous electromagnetic field was generated.

4 Conclusions

The results of this experiment are summarized as follows:

- The experiment COMET-L2 investigates the interaction of a melt with siliceous concrete in a large cylindrical cavity. The experiment aims to identify and to quantify important long-term processes at low power density (~300 kW/m^2, or ~3 MW/m^3). 430 kg steel melt plus 35 kg less dense oxide melt were poured into the concrete crucible. Unfortunately the gas measurement system failed from the beginning of the test.

- In the early phase of the test (less than 100 s), measurements show fast decrease of the melt overheat and reduction of the initially high concrete erosion rate. Concerning concrete erosion by the lower metal phase, initial erosion into axial and lateral direction is similar with an erosion ratio of ~ 1:1. For the lateral erosion by the oxide phase, the overall erosion is relatively small, so that no detailed erosion rates of the oxide can be derived. This is due to the fact that for the given conditions the temperature of the oxide melt is close to the decomposition temperature of the concrete.

- Thereafter, under stationary conditions, axial erosion is 2-3 faster than radial. Axial erosion is dominating in agreement with BETA experiments [8] at low power density.

- Reasons for the differences between axial and radial erosion following the initial transient phase, and notably also the local inhomogeneities in axial ablation, may lie in the melt heating by a planar induction coil. This technique could possibly have resulted in inhomogeneous distribution of power in the melt, with a larger proportion close to the axial ablating concrete thus promoting axial ablation. The axial ablation might have been further amplified by possible positive feedback due to progression of the erosion front towards the coils, which eventually led to the cone-shaped erosion profile [9].

- During long-term erosion, periods of moderate interaction are interrupted by short periods of significant melt eruptions. These are probably related to formation and failure of metal crusts at the cavity interface (in agreement with COMET-L1 [7]).

- Low heat fluxes to concrete result in release of unmelted aggregates / silica gravels into the melt. This may result in different heat flux distribution and erosion resulting from the lower „melting“ enthalpy of concrete, and bulk cooling of the melt by aggregates.

- Experiment approaches limits of decay heat simulation by induction heating:
    1. Further power reduction would lead to stable crusts (end of homogeneous heating of the metal phase)
    2. Metal would tend to move like a solid body.

- The test results shall be used to validate models and computer codes. Comparison with former BETA tests [8] in the low power range, such as BETA-V2.1, shows the following tendencies: The initial fast drop of the temperature of the layered melts, which is due to the high initial erosion rate, is confirmed. Comparison with high power experiments shows, however, that lateral erosion during the metal phase becomes more important when the heating power is reduced. The low power density in the present test favours the existence of metal crusts, which may have a strong influence on the shape of the cavity. Additional tests with pure oxide melts [3] are needed to complete our understanding on corium erosion.

Acknowledgements

This work has been partially sponsored by the European Commission in the 5th Framework Programme under the LACOMERA contract No. FIR1-CT2002-40158

References

[1] Miassoedov et al. Large Scale Experiments on Core Degradation, Melt Retention and Coolability (LACOMERA). FISA-2003: EU Research in Reactor Safety, Luxembourg, L, November 10-13, 2003, Preproc. p. 239-244.

[2] G.Sdouz, 2D-Behaviour of Ex-Vessel Metallic Melts Interacting with Concrete, Proposal for LACOMERA experiment, December 2003

[3] M. T. Farmer, S. Lomperski, S. Basu, Results of Reactor Materials Experiments Investigating 2-d Core-Concrete Interaction and Debris Coolability, Proc. ICAPP ’04, Pittsburgh, PA, 2004, Paper 4102.

[4] H. Alsmeyer, T. Cron, G. Messemer, W. Haefner, ECOKATS-2: A large scale experiment on melt spreading and subsequent cooling by top flooding, Proc. ICAPP ’04, Pittsburgh, PA, 2004, Paper 4134.

[5] T. Cron, G. Messemer, Internal note, January 2005.

[6] H. Alsmeyer; Internal note, January 2005.

[7] G. Doubleva, H. Alsmeyer, T. Cron, B. Fluhrer, J. Foit, G. Messemer, A. Miassoedov, S. Schmidt-Stiefel, T. Wenz, I. Ivanov, M. Cranga: COMET-L1 Test Data Report, May 2005.

[8] H. Alsmeyer; Review of Experiments on Dry Corium Concrete Interaction, in Molten corium/concrete interaction and corium coolability – A state of the art report, EUR 16649 EN,1995.

[9] M. Nie; Private communication, Framatome ANP GmbH, Oct 28, 2005.

Appendices

Appendix A: Summary of the test conditions

- **Concrete crucible**

siliceous concrete fabricated with cement of the type blast furnace cement CEM III/B 32.5 NW/HS; crucible instrumented with 90 NiCr-Ni thermocouples

- **Melt**

steel melt generated by thermite mixture (preheated to 250°C control temperature during > 36 h) and poured into concrete crucible:
460 kg Fe with 10 w% Ni
(generated oxide transferred to the slag wagon)
initial temperature of melt 1750 to 1800°C

- **Cover gas**

Ar gas flow: 50 m^3/h main flow plus 2 x 8 m^3/h from windows

- **Cameras**

on top of crucible: 1 Video (Sony), 1 Infrared camera
spout: 1 Video; end of off-gas tube: 1 Video; hall: 3 Videos

- **Induction heating**

Net power deposited in the melt: 250 kW throughout phase 1, 200 kW throughout phase 2

Initial voltage of inductor: 2.6 kV, maximum voltage 2.6 kV, reduction of voltage when heating efficiency increases after concrete erosion

- **Test procedure**

Phase 1: Dry MCCI test until –130 mm downward concrete erosion during about 25 min, detected by thermocouples
Phase 2: Subsequent reduction of heating to 200 kW until –170 mm concrete are eroded
End of heating when melt is detected by –170 mm thermocouples or upon failure of light guides. Subsequently, flooding of bottom and sidewalls of the concrete crucible to protect the test rig and to cool down the melt slowly.

- **Further details:**

Thermocouple BT 75 is defect and not registered
Light guide CX8 is defect and not activated
The turbine flow-meter is not inserted into the off-gas tube as gas flow is too low to be quantified by this technique
small Ar gas flow through porous bottom layer allows measurement of T-increase if melt approaches or penetrates lowest concrete interface.

Appendix B: Data acquisition and channel assignments

Table 11 lists all signals that are registered on the MICROLINK data acquisition system. The blocks 1, 2, 3, 5, 7, 9, and 11 of MICRLONK are equipped with high quality differential amplifiers, the blocks 4, 6, 8, 10,and 12 have ”single ended“ amplifier inputs with less noise reduction.

Table 11: COMET-L2 Meßstellenliste für Microlink-Datenerfassung

Log. Kan	HW Kan.	Block	Name	Meßgröße	Geber	Position: r,Φ,h
1	0	01:00	BT 1	Betontemperatur	NiCr/Ni	0, 0, -30
2	1	01:01	BT 2	Betontemperatur	NiCr/Ni	140, 45, -30
3	2	01:02	BT 4	Betontemperatur	NiCr/Ni	250, 45, -30
4	3	01:03	BT 5	Betontemperatur	NiCr/Ni	250, 135, -30
5	4	01:04	BT 8	Betontemperatur	NiCr/Ni	310, 45, -30
6	5	01:05	BT 9	Betontemperatur	NiCr/Ni	310, 135, -30
7	6	01:06	BT 12	Betontemperatur	NiCr/Ni	350, 45, -30
8	7	01:07	BT 14	Betontemperatur	NiCr/Ni	0, 0, -60
9	8	01:08	BT 15	Betontemperatur	NiCr/Ni	140, 45, -60
10	9	01:09	BT 17	Betontemperatur	NiCr/Ni	250, 45, -60
11	10	01:10	BT 18	Betontemperatur	NiCr/Ni	250, 135, -60
12	11	01:11	BT 21	Betontemperatur	NiCr/Ni	0, 0, -90
13	12	01:12	BT 22	Betontemperatur	NiCr/Ni	140, 45, -90
14	13	01:13	BT 24	Betontemperatur	NiCr/Ni	250, 45, -90
15	14	01:14	BT 25	Betontemperatur	NiCr/Ni	250, 135, -90
16	15	01:15	BT 28	Betontemperatur	NiCr/Ni	310, 45, -90
17	32	02:16	TE-3	TE-Ref. Modul 3	Pt 100	Mainframe
18	33	03:00	BT 29	Betontemperatur	NiCr/Ni	310, 135, -90
19	34	03:01	BT 32	Betontemperatur	NiCr/Ni	350, 45, -90
20	35	03:02	BT 38	Betontemperatur	NiCr/Ni	0, 0, -130
21	36	03:03	BT 39	Betontemperatur	NiCr/Ni	140, 45, -130
22	37	03:04	BT 41	Betontemperatur	NiCr/Ni	250, 45, -130

23	38	03:05	BT 42	Betontemperatur	NiCr/Ni	250, 135, -130
24	39	03:06	BT 46	Betontemperatur	NiCr/Ni	140, 45, -150
25	40	03:07	BT 48	Betontemperatur	NiCr/Ni	250, 45, -150
26	41	03:08	BT 49	Betontemperatur	NiCr/Ni	250, 135, -150
27	42	03:09	BT 3	Betontemperatur	NiCr/Ni	140, 225, -30
28	43	03:10	BT 6	Betontemperatur	NiCr/Ni	250, 225, -30
29	44	03:11	BT 7	Betontemperatur	NiCr/Ni	250, 315, -30
30	45	03:12	BT 10	Betontemperatur	NiCr/Ni	310, 225, -30
31	46	03:13	BT 11	Betontemperatur	NiCr/Ni	310, 315, -30
32	47	03:14	BT 13	Betontemperatur	NiCr/Ni	350, 225, -30
33	48	03:15	BT 16	Betontemperatur	NiCr/Ni	140, 225, -60
34	65	04:16	TE-5	TE-Ref. Modul 5	Pt 100	Mainframe
35	66	05:00	BT 19	Betontemperatur	NiCr/Ni	250, 225, -60
36	67	05:01	BT 20	Betontemperatur	NiCr/Ni	250, 315, -60
37	68	05:02	BT 23	Betontemperatur	NiCr/Ni	140, 225, -90
38	69	05:03	BT 26	Betontemperatur	NiCr/Ni	250, 225, -90
39	70	05:04	BT 27	Betontemperatur	NiCr/Ni	250, 315, -90
40	71	05:05	BT 30	Betontemperatur	NiCr/Ni	310, 225, -90
41	72	05:06	BT 31	Betontemperatur	NiCr/Ni	310, 315, -90
42	73	05:07	BT 33	Betontemperatur	NiCr/Ni	350, 225, -90
43	74	05:08	BT 40	Betontemperatur	NiCr/Ni	140, 225, -130
44	75	05:09	BT 43	Betontemperatur	NiCr/Ni	250, 225, -130
45	76	05:10	BT 44	Betontemperatur	NiCr/NI	250, 315, -130
46	77	05:11	BT 45	Betontemperatur	NiCr/Ni	0, 0, -150
47	78	05:12	BT 47	Betontemperatur	NiCr/Ni	140, 225, -150
48	79	05:13	BT 50	Betontemperatur	NiCr/Ni	250, 225, -150
49	80	05:14	BT 51	Betontemperatur	NiCr/Ni	250, 315, -150
50	81	05:15	BT 54	Betontemperatur	NiCr/Ni	350, 225, -150
51	98	06:16	TE-7	TE-Ref. Modul 7	Pt 100	Mainframe
52	99	07:00	BT 55	Betontemperatur	NiCr/Ni	350, 315, -150
53	100	07:01	BT 56	Betontemperatur	NiCr/Ni	0, 0, -170
54	101	07:02	RT 1	Kühlwasser ein Joche	NiCr/Ni	Jochkühlung
55	102	07:03	RT 2	Kühlwasser aus Joche	NiCr/Ni	Jochkühlung

56	103	07:04	RT 10	Rückfl.Schm.KW Nord	NiCr/Ni	Rücklaufleitung N.
57	104	07:05	BT 52	Betontemperatur	NiCr/Ni	350, 45, -170
58	105	07:06	BT 53	Betontemperatur	NiCr/Ni	350, 135, -170
59	106	07:07	BT 57	Betontemperatur	NiCr/Ni	140, 45, -170
60	107	07:08	BT 59	Betontemperatur	NiCr/Ni	250, 45, -170
61	108	07:09	BT 60	Betontemperatur	NiCr/Ni	250, 135, -170
62	109	07:10	BT 58	Betontemperatur	NiCr/Ni	140, 225, -170
63	110	07:11	BT 61	Betontemperatur	NiCr/Ni	250, 225, -170
64	111	07:12	BT 62	Betontemperatur	NiCr/Ni	250, 315, -170
65	112	07:13	BT 65	Betontemperatur	NiCr/Ni	310, 225, -170
66	113	07:14	BT 66	Betontemperatur	NiCr/Ni	310, 315, -170
67	114	07:15	BT 69	Betontemperatur	NiCr/Ni	310, 225, +290
68	131	08:16	TE-9	TE-Ref. Modul 9	Pt 100	Mainframe
69	132	09:00	BT 63	Betontemperatur	NiCr/Ni	310, 45, -170
70	133	09:01	BT 64	Betontemperatur	NiCr/Ni	310, 135, -170
71	134	09:02	BT 70	Betontemperatur	NiCr/Ni	310, 315, +290
72	135	09:03	BT 72	Betontemperatur	NiCr/Ni	310, 225, +190
73	136	09:04	BT 67	Betontemperatur	NiCr/Ni	310, 45, +290
74	137	09:05	BT 68	Betontemperatur	NiCr/Ni	310, 135, +290
75	138	09:06	BT 71	Betontemperatur	NiCr/Ni	310, 45, +190
76	139	09:07	BT 73	Betontemperatur	NiCr/Ni	330, 45, +190
77	140	09:08	BT 74	Betontemperatur	NiCr/Ni	330, 225, +190
78	141	09:09	BT 77	Betontemperatur	NiCr/Ni	310, 225, +90
79	142	09:10	RT 11	Rückfl. Schm.KW Süd	NiCr/Ni	Rücklaufleitung S.
80	143	09:11	BT 80	Betontemperatur	NiCr/Ni	330, 225, +90
81	144	09:12	IR 1	Temperatur IR Objektiv	NiCr/Ni	310, 45, +100
82	145	09:13		Microlink Kanal defekt		
83	146	09:14	BT 79	Betontemperatur	NiCr/Ni	350, 45, +90
84	147	09:15	KT 10	Temp. Gießrinne	W3Re/25	
85	164	10:16	TE-11	TE-Ref. Modul 11	Pt 100	Mainframe
86	165	11:00	BT 76	Betontemperatur	NiCr/Ni	310, 135, +90
87	166	11:01		nicht belegt		
88	167	11:02	BT 78	Betontemperatur	NiCr/Ni	310, 315, +90

89	168	11:03		nicht belegt		
90	169	11:04		nicht belegt	Pt10Rh/Pt	
91	170	11:05	CT 1	GFK-Rohr-Temp. Innen	NiCr/Ni	571, 135
92	171	11:06	CT 2	GFK-Rohr-Temp. Innen	NiCr/Ni	571, 45
93	172	11:07	CT 3	GFK-Rohr-Temp. Innen	NiCr/Ni	571, 315
94	173	11:08	CT 4	GFK-Rohr-Temp. Innen	NiCr/Ni	571, 225
95	174	11:09	BT 35	Betontemperatur	NiCr/Ni	380, 135, -90
96	175	11:10	BT 34	Betontemperatur	NiCr/Ni	380, 45, -90
97	176	11:11	BT 37	Betontemperatur	NiCr/Ni	380, 315, -90
98	177	11:12	BT 36	Betontemperatur	NiCr/Ni	380, 225, -90
99	178	11:13	KM 1	Einguss - Masse	Waage	Reaktionstiegel
100	179	11:14	BT 83	Betontemperatur	NiCr/Ni	310, 225, +15
101	180	11:15	BT 84	Betontemperatur	NiCr/Ni	310, 315, +15
102	197	12:16	TE-13	TE-Ref. Modul 13	Pt 100	Mainframe
103	16	02:00	BT 86	Betontemperatur	NiCr/Ni	330, 225, +15
104	17	02:01	BT 89	Betontemperatur	NiCr/Ni	380, 225, +15
105	18	02:02	BT 81	Betontemperatur	NiCr/Ni	310, 45, +15
106	19	02:03	BT 90	Betontemperatur	NiCr/Ni	380, 315, +15
107	20	02:04	BT 82	Betontemperatur	NiCr/Ni	310, 135, +15
108	21	02:05	BT 85	Betontemperatur	NiCr/Ni	330, 45, +15
109	22	02:06	WP 10	Wasserdruck	DMS	Tiegel-SW
110	23	02:07	BT 87	Betontemperatur	NiCr/Ni	380, 45, +15
111	24	02:08	WP 15	Wasserdruck	DMS	W-Zulauf
112	25	02:09	HP 1	Hauben-Druck	DMS	0 - 2 bar absolut
113	26	02:10	HP 2	Hauben Druck	DMS	0 - 10 bar diff.
114	27	02:11	BT 88	Betontemperatur	NiCr/Ni	380, 135, +15
115	28	02:12	AR 1	Frequenz	AEG 13	1,2,W+X
116	29	02:13	AN 3	Leistung Umrichter 3	AEG 5	1,2,C+D
117	30	02:14	AN 4	Leistung Umrichter 4	AEG 7	1,2,H+I
118	31	02:15	AU 2	Anl. Spannung 3000 V	AEG 10	1,2,P+R
119	49	04:00				
120	50	04:01				
121	51	04:02				

122	52	04:03				
123	53	04:04	GC 11	Gas-M., INR 1	Q 100-1	
124	54	04:05	GC 12	Gas-M., INR 2	Q 100-1	
125	55	04:06	GC 13	Gas-M., INR 3	Q 100-1	
126	56	04:07	GC 14	Gas-M., INR 4	Q 100-1	
127	57	04:08	GC 15	Gas-M., INR 5	Q 100-1	
128	58	04:09	GC 16	Gas-M., INR 6	Q 100-1	
129	59	04:10	GC 17	Gas-M., INR 7	Q 100-1	
130	60	04:11	GC 18	Gas-M., INR 8	Q 100-1	
131	61	04:12	GX 1	Empf., INR 9	Q 100-1	
132	62	04:13	GC 10	Gas-Scan, INR 10	Q 100-1	
133	63	04:14	GC 21	Gas-M., INR 11	Q 100-2	
134	64	04:15				
135	82	06:00	GC 22	Gas-M., INR 12	Q 100-2	
136	83	06:01	GC 23	Gas-M., INR 13	Q 100-2	
137	84	06:02	GC 24	Gas-M., INR 14	Q 100-2	
138	85	06:03	GC 25	Gas-M., INR 15	Q 100-2	
139	86	06:04	GC 26	Gas-M., INR 16	Q 100-2	
140	87	06:05	GC 27	Gas-M., INR 17	Q 100-2	
141	88	06:06	GC 28	Gas-M., INR 18	Q 100-2	
142	89	06:07	GX 2	Empfindl., INR 19	Q 100-2	
143	90	06:08		Ind. -Bruttoleistung		Intern berechnet
144	91	06:09	SN 1	Ind. -Nettoleistung		Intern berechnet
145	92	06:10	AU 2	Ind. -Spannung		Intern berechnet
146	93	06:11	AR 1	Ind. -Frequenz		Intern berechnet
147	94	06:12				
148	95	06:13	AA 3	Strom Umrichter 3	AEG 14	1,2,F,E
149	96	06:14				
150	97	06:15				
151	115	08:00	AA 4	Strom Umrichter 4	AEG 8	1,2,K+L
152	116	08:01	AU 1	Umr. Spannung 1000 V	AEG 9	1,2,M+N
153	117	08:02				
154	118	08:03	AA 5	Kond. Teilstrom A	AEG 11	1,2,S+T

155	119	08:04	AA 6	Kond. Teilstrom B	AEG 12	1,2,U+V
156	120	08:05				
157	121	08:06	RF 1	Rückkühlanlage	Wirbelm.	Durchfluß
158	122	08:07				
159	123	08:08				
160	124	08:09		GQ 22	Hygrom. 2	
161	125	08:10		GT 22	Hygrom. 2	
162	126	08:11	GF 1	Gasvolumen	Flügelrad	
163	127	08:12	GP 1	Gasdruck	DMS	bei Meßdüse
164	128	08:13	RQ 1	Leistung Rückkühl-Anl.	RF1,Pt100	Rückkühlanlage
165	129	08:14	SN 3	Pultanzeige Nettoleistg.		Nettoleistung
166	130	08:15				
167	148	10:00	AP 1	Ar-Druck	DMS	Haube ein
168	149	10:01	AP 2	Ar-Druck	DMS	Ar-Batterie
169	150	10:02	AP 3	Ar-Druck	DMS	Periskop Kühlg.
170	151	10:03	AF 1	Ar-Strom	RotaM ?	Haube ein
171	152	10:04	AF 2	Ar-Strom	Meßblende	Periskop Freibl.
172	153	10:05		GQ 21	Hygrom. 1	
173	154	10:06		GT 21	Hygrom. 1	
174	155	10:07				
175	156	10:08				
176	157	10:09	HP 3	Hauben-Druck	DMS	0 - 100 bar diff.
177	158	10:10	AF 4	Ar-Strom	Meßblende	Aerosol-Spülung
178	159	10:11	AF 3	Ar-Strom	Meßblende	Periskop Kühlg.
179	160	10:12	AE 1	Ereignis	Logik	Zündg., Abstich
180	161	10:13				
181	162	10:14	CK 1	Zeitmarke	Clock	Synchronisation
182	163	10:15				
183	181	12:00	HT 1	Hauben Temp.	NiCr/Ni	Haubenflansch
184	182	12:01	GT 1	Gastmp. n. Abscheider	NiCr/Ni	n. Abscheider
185	183	12:02	GT 2	Gastemp. b. Meßdüse	NiCr/Ni	bei Meßdüse
186	184	12:03	KT 1	Wandtemp. Absch.	NiCr/Ni	Abscheider
187	185	12:04	KT 2	Wandtemp. b. Meßd.	NiCr/Ni	bei Meßdüse

188	186	12:05	KT 3	Zuluft-Temp.	NiCr/Ni	Lüftg. Mitte
189	187	12:06	KT 4	Hallentemp.	Pt 100	
190	188	12:07				
191	189	12:08				
192	190	12:09	GP 2	Staurohrmessung	Diff. Druck	bei Meßdüse
193	191	12:10	CL 1	Wasserstand Tiegel	Druck	Tiegel-N
194	192	12:11	WF 16	Wasserdurchfluß	magn.-ind.	W-Zulauf
195	193	12:12	WF 17	Wasserd.fl. Notkühlung	magn.-ind.	Tiegelhaube
196	194	12:13	KU 1	Kontr.Spannung	0 mV	
197	195	12:14	KU 2	Kontr.Spannung	40 mV	
198	196	12:15	LV 115	Steuerung WF 15	Ventil 115	W-Zulauf

* Verstärker berücksichtigt bereits Kartentemperatur

BT 75, NiCr/Ni (310, 45, 100) Log Kanal 81, vor Versuch defekt

Nachträglich Kanal 81 mit IR 1 belegt (Temp. IR-Objektiv)

Appendix C: Test data

This appendix provides plots showing the temperature rise in the concrete and the failure of the thermocouples. The thermocouples are grouped according to show the progression of the melt in the concrete.

In addition, the plot of the constant argon cover gas flow is shown.

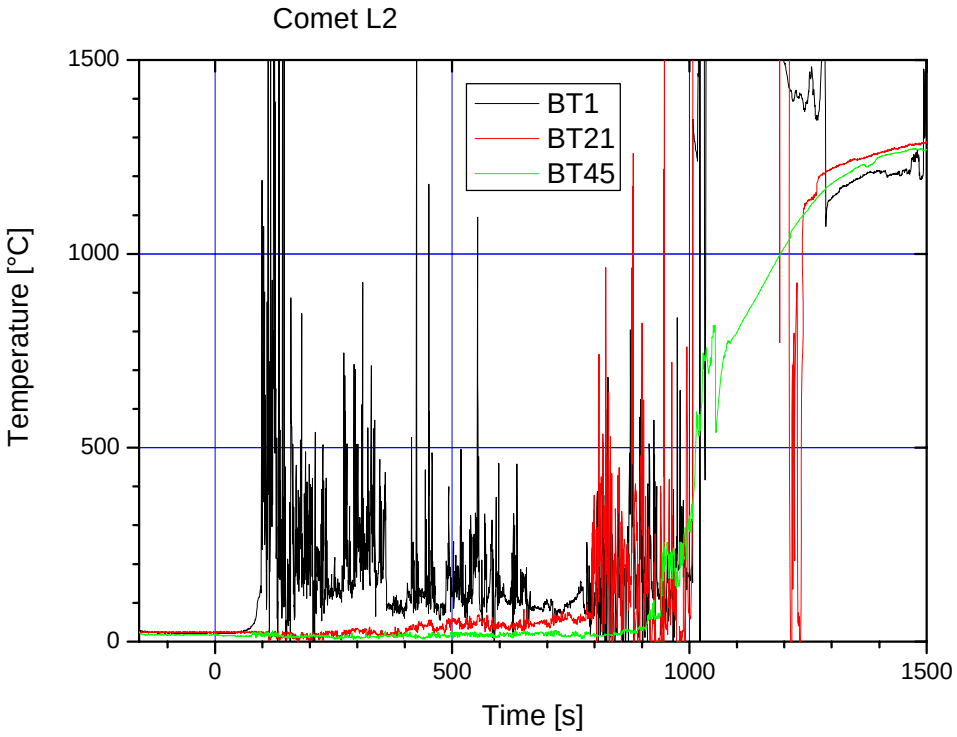

Figure 29: Thermocouples on the centre line BT 1, BT 21, and BT 45

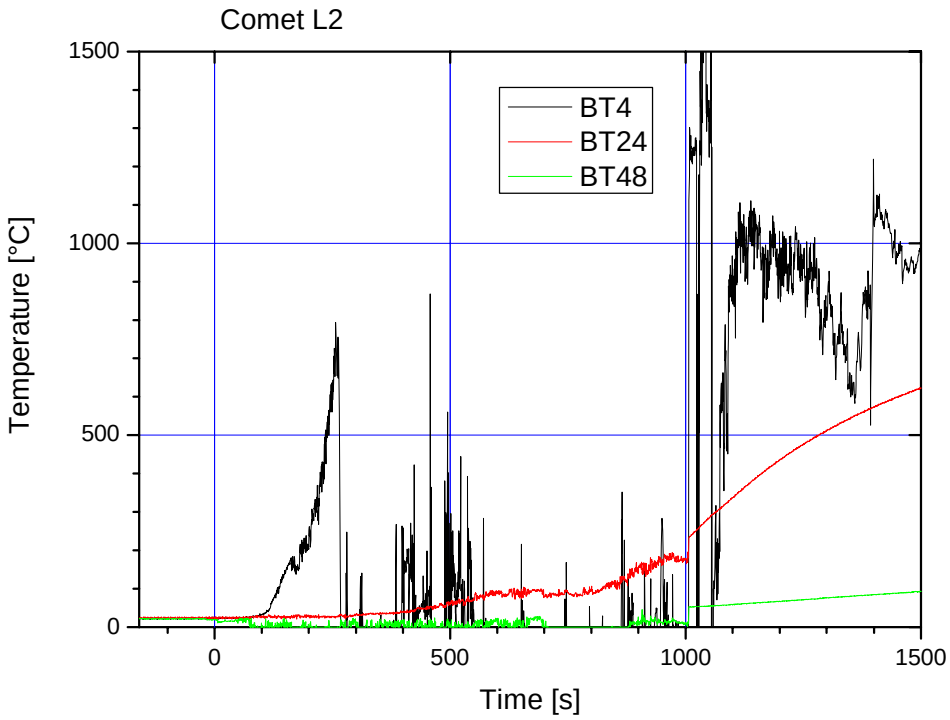

Figure 30: Thermocouples BT 4, BT 24, and BT 48

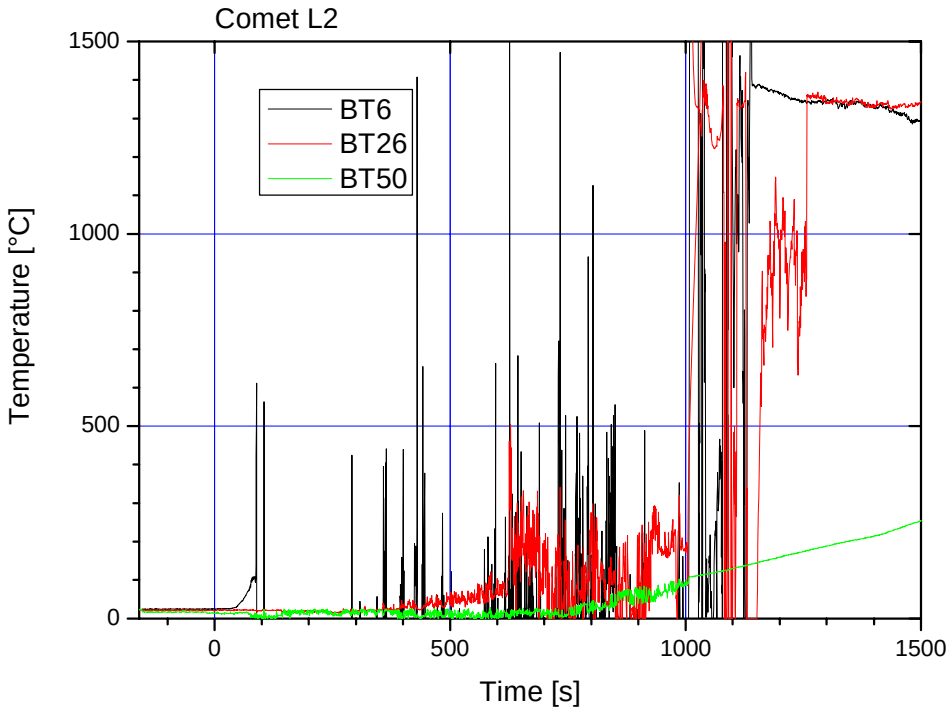

Figure 31: Thermocouples BT 6, BT 26, and BT 50

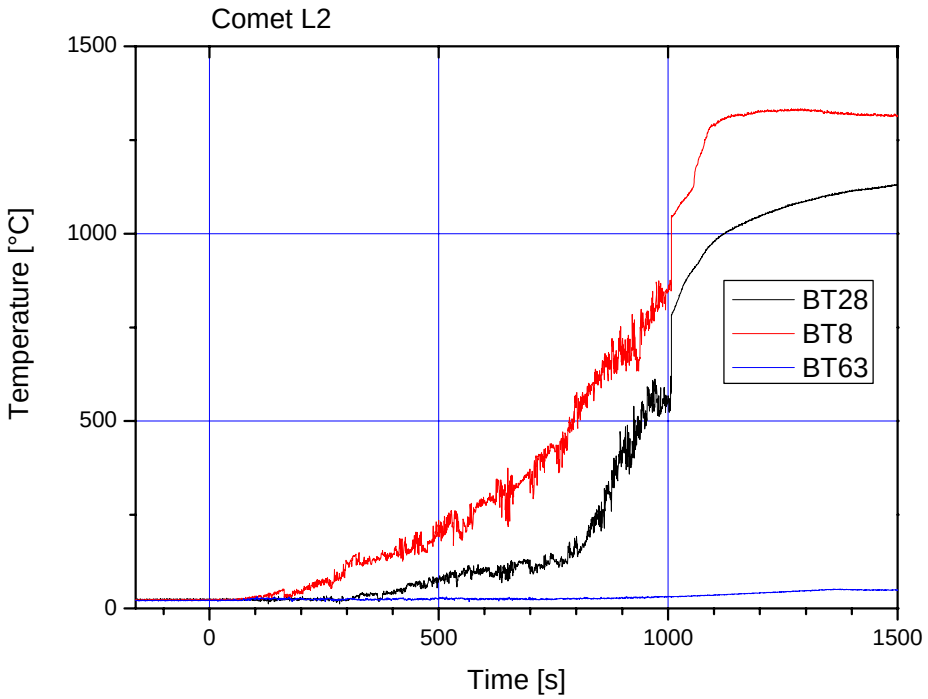

Figure 32: Thermocouples BT 8, BT 28, and BT 63

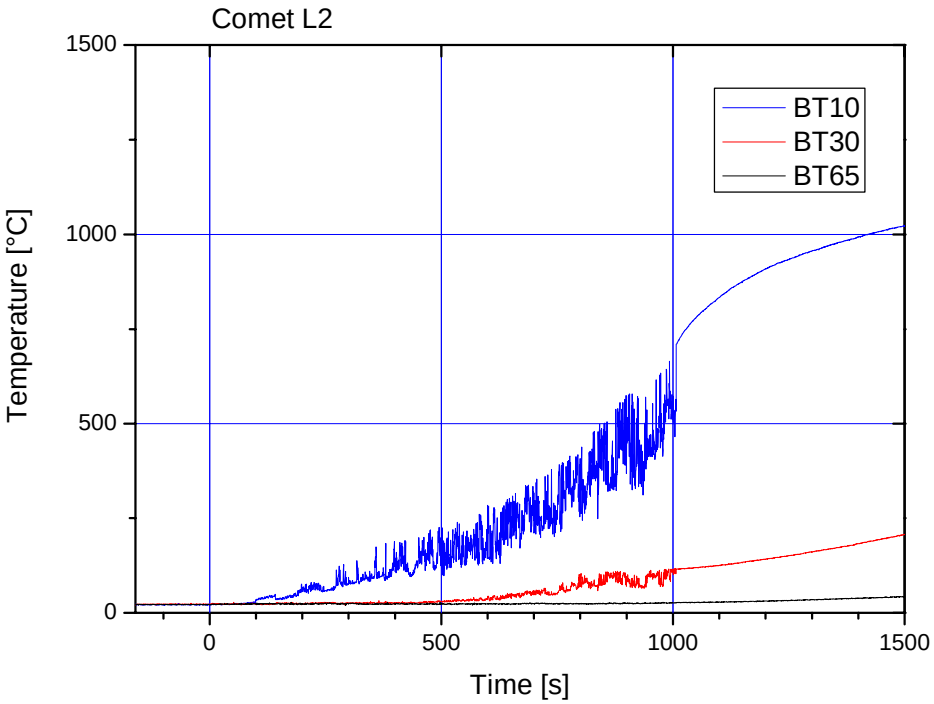

Figure 33: Thermocouples BT 10, BT 30, and BT 65

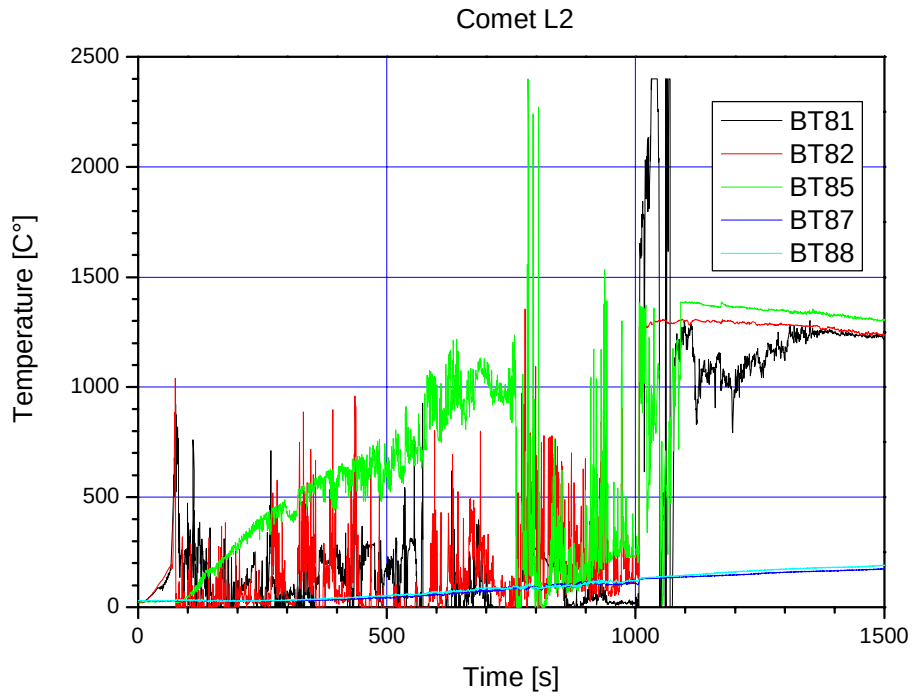

Figure 34: Thermocouples BT 81, BT 85, BT 87, BT 82 and BT 88

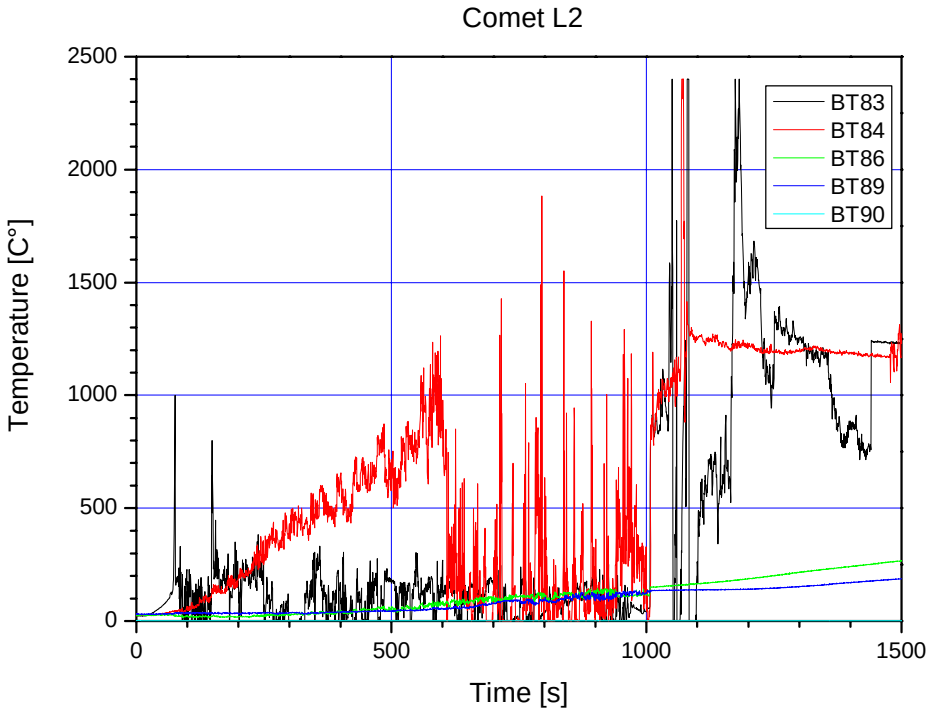

Figure 35:Thermocouples BT 89, BT 83, BT 86, BT 90, and BT 84

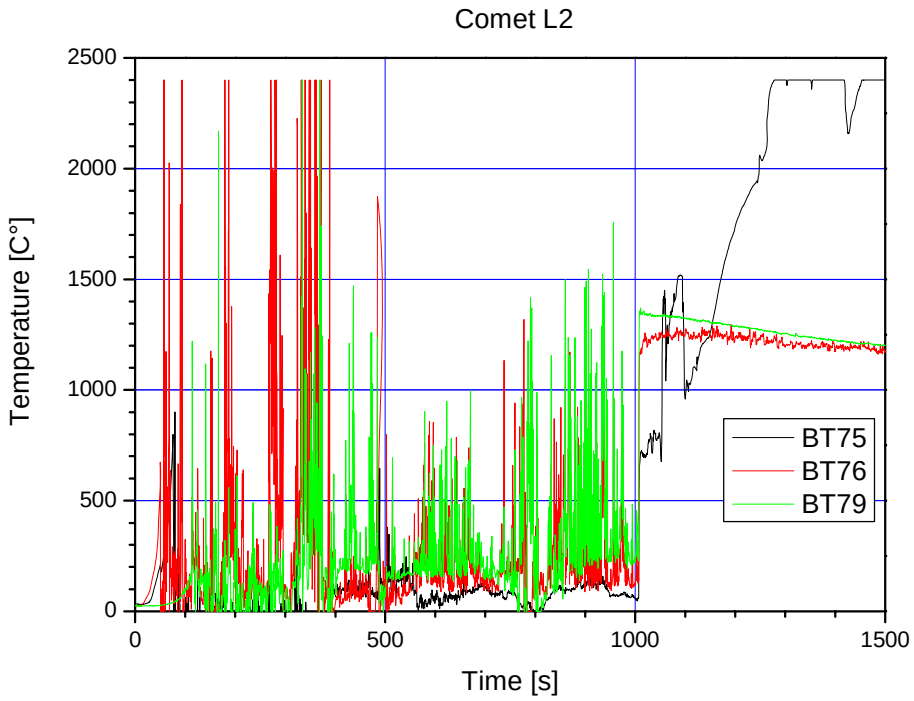

Figure 36: Thermocouples BT 75, BT 76, and BT 79

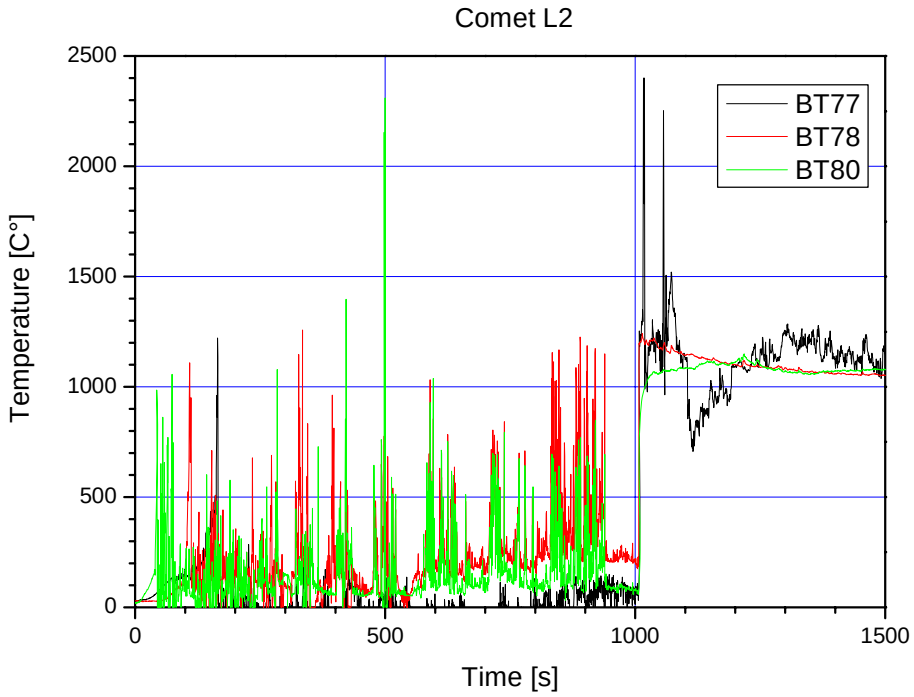

Figure 37: Thermocouples BT 80, BT 77, and BT 78

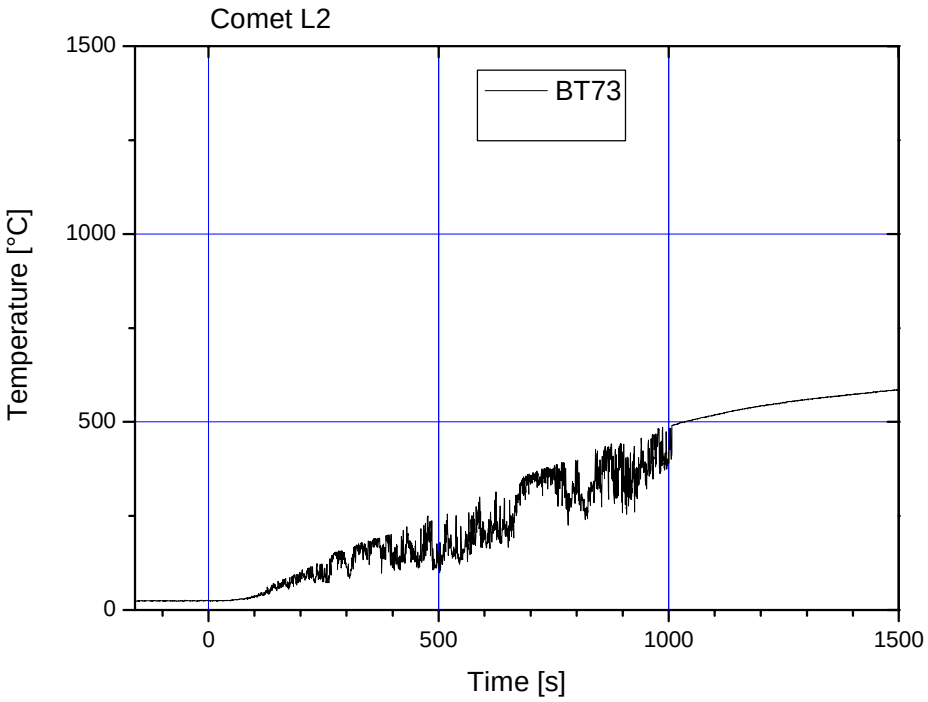

Figure 38: Thermocouples BT 41, BT 69, and BT 87

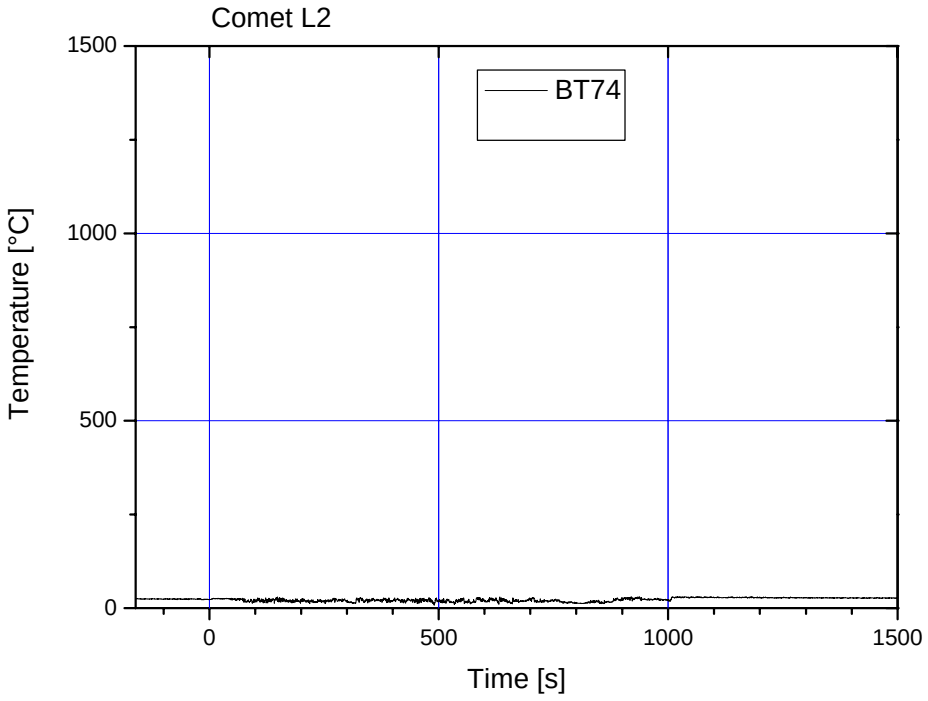

Figure 39: Thermocouples BT 74

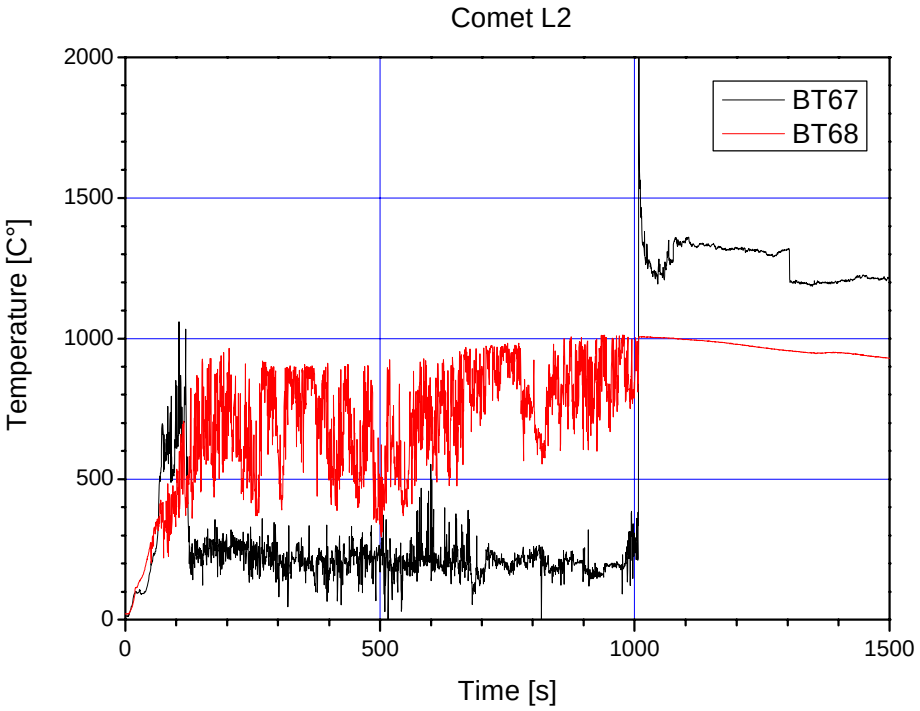

Figure 40: Thermocouples BT 67 and BT 68

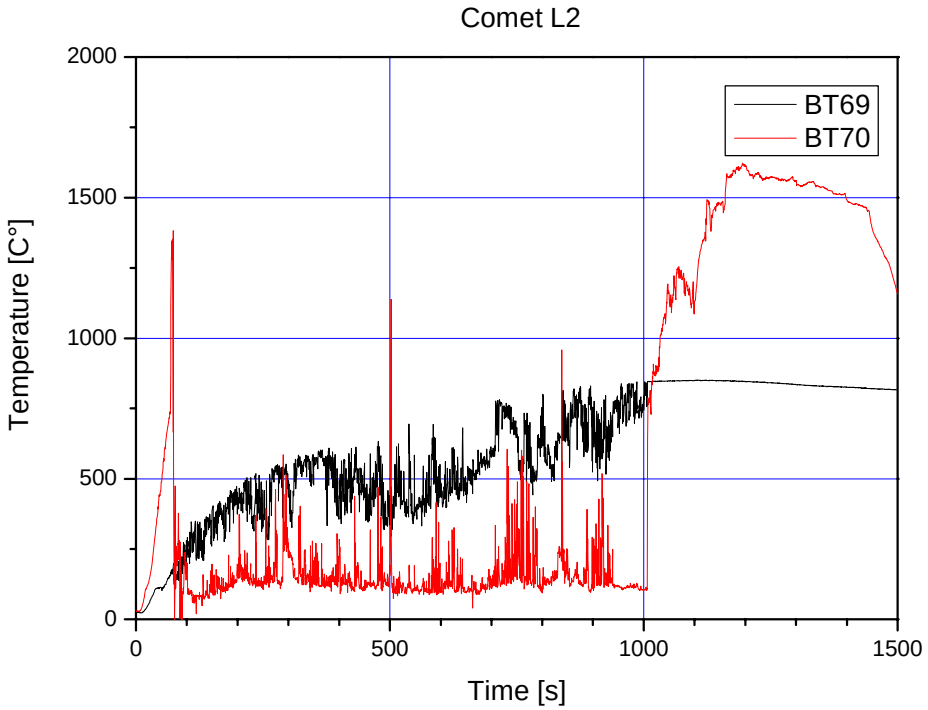

Figure 41: Thermocouples BT 69 and BT 70

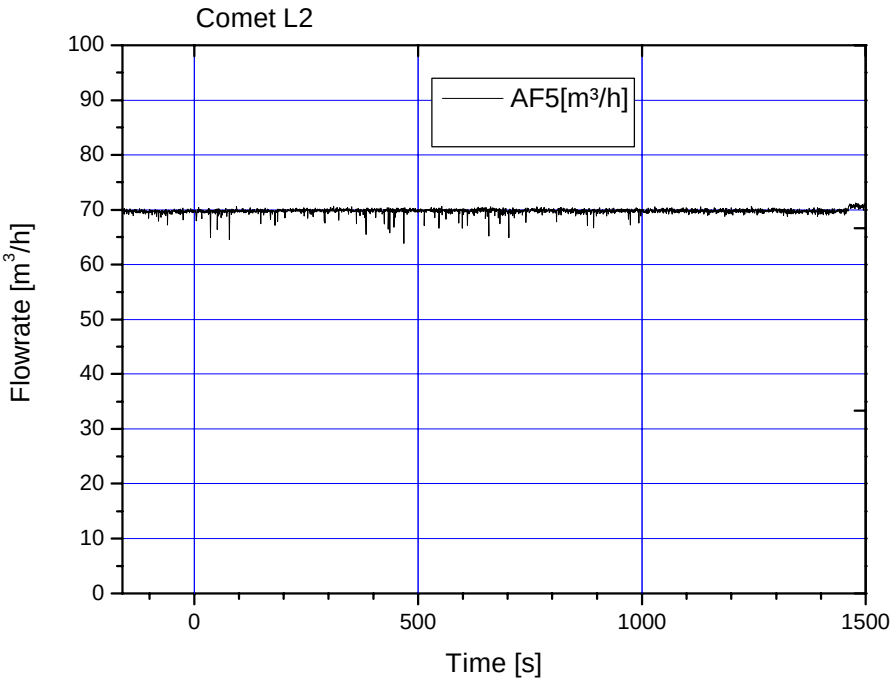

Figure 42: Argon flow in the off-gas tube